GluN2A NMDA Receptor Enhancement Improves Brain Oscillations, Synchrony, and Cognitive Functions in Dravet Syndrome and Alzheimer's Disease Models

Jesse E. Hanson[1,8,9,*], Keran Ma[6,7,8], Justin Elstrott[2,8], Martin Weber[1,8], Sandrine Saillet[6,7,8], Abdullah S. Khan[6], Jeffrey Simms[6], Benjamin Liu[6], Thomas A. Kim[6], Gui-Qiu Yu[6], Yelin Chen[1], Tzu-Ming Wang[1], Zhiyu Jiang[1], Bianca M. Liederer[3], Gauri Deshmukh[3], Hilda Solanoy[1], Connie Chan[4], Benjamin D. Sellers[5], Matthew Volgraf[5], Jacob B. Schwarz[5], David H. Hackos[1], Robby M. Weimer[1,2], Morgan Sheng[1], T. Michael Gill[6], Kimberly Scearce-Levie[1], Jorge J. Palop[6,7,*]

[1]Department of Neuroscience, Genentech Inc., South San Francisco, CA 94080, USA

[2]Department of Biomedical Imaging, Genentech Inc., South San Francisco, CA 94080, USA

[3]Department of Drug Metabolism and Pharmacokinetics, Genentech Inc., South San Francisco, CA 94080, USA

[4]Department of Pharmaceuticals, Genentech Inc., South San Francisco, CA 94080, USA

[5]Department of Discovery Chemistry, Genentech Inc., South San Francisco, CA 94080, USA

[6]Gladstone Institute of Neurological Disease, San Francisco, CA 94158, USA

[7]Department of Neurology, University of California, San Francisco, San Francisco, CA 94158, USA

[8]These authors contributed equally

[9]Lead Contact

SUMMARY

NMDA receptors (NMDARs) play subunit-specific roles in synaptic function and are implicated in neuropsychiatric and neurodegenerative disorders. However, the *in vivo* consequences and

therapeutic potential of pharmacologically enhancing NMDAR function via allosteric modulation are largely un-known. We examine the *in vivo* effects of GNE-0723, a positive allosteric modulator of GluN2A-subunit-containing NMDARs, on brain network and cognitive functions in mouse models of Dravet syndrome (DS) and Alzheimer's disease (AD). GNE-0723 use dependently potentiates synaptic NMDA receptor currents and reduces brain oscillation power with a predominant effect on low-frequency (12–20 Hz) oscillations. Interestingly, DS and AD mouse models display aberrant low-frequency oscillatory power that is tightly correlated with network hypersynchrony. GNE-0723 treatment reduces aberrant low-frequency oscillations and epileptiform discharges and improves cognitive functions in DS and AD mouse models. GluN2A-subunit-containing NMDAR enhancers may have therapeutic benefits in brain disorders with network hypersynchrony and cognitive impairments.

Graphical Abstract
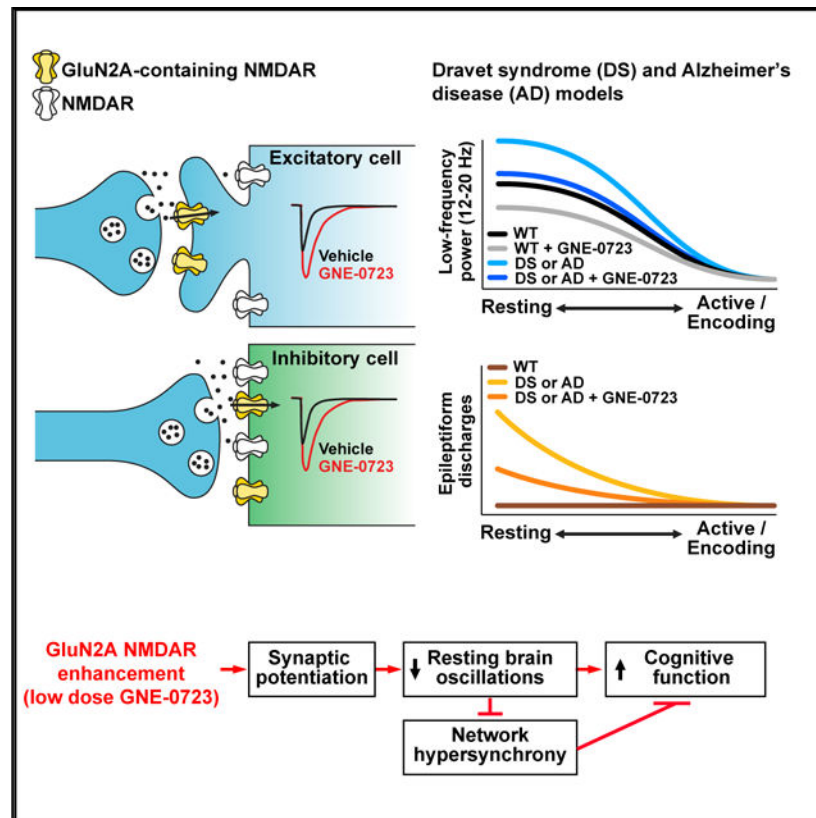
In Brief

Hanson et al. examine the therapeutic effects of enhancing GluN2A-subunit-containing NMDAR function in Dravet syndrome and Alzheimer's disease mice. GNE-0723 treatment reduces aberrant low-frequency oscillations and epileptiform discharges and improves cognitive functions in both disease models. GluN2A NMDAR enhancers may benefit brain disorders with network hypersynchrony and cognitive impairments.

INTRODUCTION

NMDA receptors (NMDARs) are ionotropic glutamate receptors that play key roles in synaptic plasticity and are implicated in neurological disorders (Paoletti et al., 2013; Traynelis et al., 2010). NMDARs are tetrameric; composed of GluN1, GluN2A-D, and GluN3A-B subunits; and typically consist of two GluN1 subunits and two GluN2 subunits in adult animals (Kehoe et al., 2013; Paoletti et al., 2013; Traynelis et al., 2010). In pyramidal cells, synaptic NMDARs typically contain GluN2A subunits, display faster kinetics, and mediate long-term synaptic plasticity, whereas extrasynaptic NMDARs typically lack GluN2A subunits, contain mainly GluN2B subunits, and display slower kinetics.

Until recently, insight into the *in vivo* function of NMDARs has come mostly from pharmacological modulation of NMDARs with limited synaptic and NMDAR-subunit selectivity, mainly using antagonists, such as ketamine, memantine, or MK-801. Treatment with these NMDAR blockers induces a schizophrenia-like syndrome in humans (Javitt and Zukin, 1991; Krystal et al., 1994; Rivolta et al., 2015) and rodents (Zajaczkowski et al., 2003), including locomotor hyperactivity, aberrant electroencephalogram (EEG) oscillatory activity, and cognitive impairments. Although NMDARs are found on inhibitory and excitatory neurons, it has been proposed that the underlying mechanism of the *in vivo* effects of NMDAR blockers involves reduction of inhibitory interneuron activation, leading to dis-inhibition of pyramidal cells and increased cortical excitability (Gonzalez-Burgos and Lewis, 2012; Miller et al., 2016; Picard et al., 2019; Sapkota et al., 2016). Consistently, inhibition of NMDARs by MK-801 causes a reduction in the firing rate of fast-spiking interneurons and a subsequent increase in pyramidal cell firing rates in awake rats (Homayoun and Moghaddam, 2007). The preferential impact of NMDAR antagonists on fast-spiking interneurons *in vivo* is thought to result from greater basal NMDAR activation in interneurons due to their higher rate of firing and more depolarized membrane potential, which relieves pore block by Mg^{2+} (Cohen et al., 2015). A preferential effect of NMDAR antagonists on the parvalbumin (PV) interneuron-enriched GluN2D subunit under physiological conditions could also contribute (Kotermanski and Johnson, 2009; Perszyk et al., 2016). Notably, GluN2D knockout mice or mice with global or PV interneuron-specific knockout of GluN2A lack ketamine-induced, schizophrenia-related phenotypes, including hyperlocomotion and excessive gamma oscillatory activity (Picard et al., 2019; Sapkota et al., 2016).

Although the functional roles of synaptic and extrasynaptic NMDARs in health and disease are not fully understood, extrasynaptic GluN2B-containing NMDARs may mediate neurotoxicity in Alzheimer's disease (AD) pathogenesis and other brain disorders (Hu et al., 2009; Li et al., 2011; Mony et al., 2009; Snyder et al., 2005; Um et al., 2012). Interestingly, the NMDAR antagonist memantine, which is used to treat moderate-to-severe AD, might exert neuroprotection by blocking aberrant activation of extrasynaptic GluN2B-containing NMDARs but may also block synaptic NMDAR function (Hardingham et al., 2002; Lipton, 2005; Papadia and Hardingham, 2007; Xia et al., 2010; Zhou and Sheng, 2013). Therefore, GluN2A-containing NMDARs represent an attractive and complementary target for selectively enhancing synaptic NMDAR function while avoiding extrasynaptic neurotoxicity.

Toward this goal, selective positive allosteric modulators (PAMs) of GluN2A-subunit-containing NMDARs (GluN2A PAMs) have been identified (Hackos et al., 2016). Unlike agonists, GluN2A PAM compounds enhance synaptic NMDAR currents only when and where NMDARs are naturally activated by synaptic glutamate release and therefore selectively enhance endogenous NMDAR activity. Given that NMDAR antagonists predominantly increase network hypersynchrony *in vivo*, drugs that enhance the function of synaptic NMDARs may potentially be beneficial in suppressing pathological hypersynchrony. However, in contrast to the extensive data on NMDAR antagonists, little is known about the *in vivo* consequences of pharmacologically enhancing NMDAR function or the therapeutic potential of this approach.

Reduced interneuron function and pathological network hypersynchrony have been implicated in neuropsychiatric and neurodegenerative disorders, including schizophrenia, Dravet syndrome (DS), and AD. DS is a genetic epileptic encephalopathy often caused by *de novo* nonsense mutations in the SCN1A gene, resulting in haploinsufficiency of the voltage-gated sodium channel Nav1.1 (Catterall et al., 2010). Nav1.1 is predominantly expressed in medial ganglionic eminence (MGE)-derived inhibitory interneurons, which have proportionally higher Nav1.1 levels relative to other Nav subunits (Saunders et al., 2018). Fast-spiking action potential activity is also associated with higher levels of Nav1.1 and lower levels of Nav1.2 (Saunders et al., 2018). Nav1.1-deficient mice have selective reductions in both PV and somatostatin interneuron action potential firing rates that are thought to contribute to the epileptic phenotypes (Catterall et al., 2010; Martinez-Losa et al., 2018; Ogiwara et al., 2007; Rubinstein et al., 2015; Tai et al., 2014; Yamakawa, 2009; Yu et al., 2006). Nav1.1 levels are also reduced in mouse models of AD, including J20, APP/PS1, and TgCRND8 mice, and in humans with AD (Hamm et al., 2017; Hu et al., 2017; Verret et al., 2012). Beta-secretase (BACE)-1-dependent Nav1.1 hypofunction has also been suggested in Tg2576 and BACE1 transgenic mice (Corbett et al., 2013; Kim et al., 2007). Thus, interneuron hypofunction may contribute to network hypersynchrony and oscillatory alterations in mouse models of DS and AD.

Previously developed GluN2A PAMs, including GNE-6901 and GNE-8324 (Hackos et al., 2016), had unfavorable pharmacokinetic (PK) properties that prevented evaluation of their potential therapeutic effects in relevant disease models *in vivo*. In this study, we use GNE-0723, a related GluN2A PAM with high potency and favorable PK properties (Volgraf et al., 2016), to explore the functional consequences of enhancing synaptic NMDAR function *in vivo*. High GNE-0723 doses caused behavioral changes in wild-type, but not in GluN2A knockout (KO), mice that were contrary to the effects of NMDAR antagonists, suggesting that GNE-0723 specifically enhances GluN2A-containing NMDAR function *in vivo*. We proceeded to test the therapeutic effects of GNE-0723 treatment in DS and AD mouse models, which exhibit altered oscillatory activity, network hypersynchrony, and behavioral alterations. Treatment with a low dose of GNE-0723 reduced aberrant low-frequency (12–20 Hz) oscillatory activity, network hypersynchrony, and cognitive impairment in DS and AD mouse models. Our results demonstrate the potential therapeutic benefit of enhancing GluN2A-containing NMDARs in brain disorders with impaired inhibitory function, network hypersynchrony, and cognitive impairments, including DS and AD.

RESULTS

GNE-0723 Is a GluN2A PAM with Appropriate Properties for *In vivo* Use

GNE-0723 potentiates recombinant GluN2A-containing NMDARs with an EC_{50} of approximately 20 nM and at least 250-fold selectivity against GluN2B-containing NMDARs and AMPARs in cell-based assays (Hackos et al., 2016). Whole-cell recordings at room temperature (RT) from cell lines expressing GluN2A-containing NMDARs showed that 1 μM GNE-0723 enhanced the peak current and slowed the current deactivation in response to brief pulses of glutamate (Glu) (Figures 1A, 1B, and S1). GNE-0723 at 1 μM enhanced NMDAR currents evoked by a wide range of Glu concentrations (0.03–100 μM), which was reflected in a significant lowering of the Glu EC_{50} in the presence of GNE-0723 (Figures 1A and 1C). GNE-0723 potentiation of NMDAR currents was equally robust when tested at RT or 37°C (Figure S1).

Single oral dosing of 1, 3, and 10 mg/kg of GNE-0723 in wild-type mice resulted in dose-linear plasma concentrations with respective calculated unbound Cmax concentrations of 5, 12, and 46 nM (Figure 1D). Low clearance was observed for GNE-0723, with stable plasma and brain levels maintained for at least 24 h following dosing with 3 mg/kg GNE-0723 (Figures 1D and 1E). GNE-0723 also showed excellent brain penetration, reflecting a lack of active efflux with similar unbound plasma and brain GNE-0723 concentrations during the 24 h post-dose (Figure 1E). In contrast to GNE-0723, previously reported GluN2A PAMs, GNE-6901 and GNE-8324 (Hackos et al., 2016), were rapidly cleared and did not achieve physiologically relevant concentrations after oral dosing (Volgraf et al., 2016).

We next tested GNE-0723 under more physiologically relevant conditions using piezoelectric solution switching to allow repeated synaptic-like Glu applications (5 ms; 100 μM). Under these conditions, the prominent effect of 30 nM GNE-0723 was to slow deactivation of the NDMAR current rather than enhance peak current (Figure 1F). Repeated Glu applications at 30-s or 90-s intervals in the presence of GNE-0723 resulted in use-dependent potentiation of GluN2A-containing NMDARs currents (Figures 1G and 1H), suggesting active synapses *in vivo* may potentially undergo a similar use-dependent potentiation.

GNE-0723 Potentiates NMDAR EPSCs in Excitatory and Inhibitory Neurons *Ex Vivo*

We previously found that distinct GluN2A PAMs, GNE-6901 and GNE-8324, greatly vary in their ability to potentiate NMDARs currents at synapses (Hackos et al., 2016). Therefore, we tested the ability of GNE-0723 to potentiate evoked NMDAR excitatory postsynaptic currents (EPSCs) in cortical pyramidal neurons and inhibitory interneurons in brain slices from adult mice. GNE-0723 application at 0.3 and 1.0 μM robustly increased the peak (196% ± 68%; $p < 0.05$ and 243% ± 62%; $p < 0.05$, respectively), area (289% ± 112%; $p < 0.05$ and 419% ± 147%; $p < 0.05$), and decay time (177% ± 28%; $p < 0.001$ and 244% ± 80%; $p < 0.05$) of evoked NMDAR EPSCs in pyramidal neurons (Figures 2A, 2C, and 2E), demonstrating the ability of GNE-0723 to potentiate native synaptic NMDARs in brain slices. Next, we tested for GNE-0723 effects on evoked NMDAR EPSCs recorded from PV-positive interneurons that were identified using a fluorescent reporter driven by PV-cre

recombinase expression. Similar to pyramidal neurons, 0.3 and 1.0 mM GNE-0723 also showed a robust potentiation of the peak (152% ± 32%; p = 0.06 and 155% ± 36%; p < 0.05), area (194% ± 52%; p < 0.05 and 275% ± 77%; p < 0.05), and decay time (124% ± 11%; p < 0.05 and 208% ± 36%; p < 0.001) of evoked NMDAR EPSCs in PV-positive interneurons (Figures 2B, 2D, and 2F). Consistent with use-dependent potentiation of recombinant NMDARs by GNE-0723 (Figures 1G, 1H, and S1), there was a relatively slow onset of GNE-0723 potentiation in both pyramidal neurons and PV interneurons in brain slices during stimulation with a 30-s inter-stimulus interval. Because synaptic NMDARs on both excitatory and inhibitory neurons could be robustly potentiated under these *ex vivo* conditions, it is reasonable to speculate that both excitatory and inhibitory cells could contribute to the *in vivo* effects of GNE-0723.

GNE-0723-Induced Behavioral Changes Depend on GluN2A-Containing NMDARs

Because NMDAR antagonists cause hyperlocomotion in mice (Zajaczkowski et al., 2003), we reasoned that enhancing GluN2A-containing NMDAR function with GNE-0723 may cause hypoactivity. As previously described (Dravid et al., 2007), we observed dose-dependent increases in locomotor activity by (+)-MK-801 in wild-type (WT) mice (Figure S2A). (+)-MK-801 caused hyperactivity at a dose at which the less-potent enantiomer (−)-MK-801 had no effects (Figure S2B), indicating that these behavioral effects were mediated by NMDAR blockade. In contrast, high doses of GNE-0723 suppressed ambulatory locomotor activity (10 mg/kg) and rearings (6 and 10 mg/kg) in WT mice, whereas the lower 3-mg/kg dose had no effects on ambulatory locomotor activity and a trend toward reduced rearings (Figures 3A and 3B).

To determine whether GNE-0723-induced behavioral effects are mediated by GluN2A-containing NMDARs, we next examined the locomotor effects of acute GNE-0723 treatment in GluN2A knockout (GluN2A[KO]) mice. As previously observed, and consistent with NMDA hypofunction (Boyce-Rustay and Holmes, 2006), GluN2A[KO] mice exhibited increased basal ambulatory locomotor activity compared to WT mice (Figures S2C, 3A, and 3C). In contrast to WT mice, GNE-0723 at 3, 6, and 10 mg/kg did not alter ambulatory locomotor activity or rearings in GluN2A KO mice (Figures 3C and 3D). These results indicate that GNE-0723-induced behavioral changes are mediated by GluN2A-containing NMDARs.

GluN2A-Containing NMDARs Modulate Network Oscillatory Activity in Behaving Mice

Changes in brain network oscillatory activity correlate with psychiatric symptoms, epileptiform activity, and cognitive performance in psychiatric and neurological disorders (Palop and Mucke, 2016). To examine the impact of GluN2A-containing NMDARs modulation on brain function and its potential therapeutic profile, we first determined the effects of GNE-0723 on brain network oscillations during active wake and NREM by EEG recordings and compared its oscillatory profile to the pro-psychotic NMDAR blocker (+)-MK-801. At the lower 3-mg/kg dose, GNE-0723 selectivity reduced the power of low-frequency oscillations within the 12- to 20-Hz band (alpha and low beta), but not within the delta (0.5–6 Hz), theta (6–10 Hz), or gamma (30–80 Hz) bands, during active wake and NREM (Figures 3E, 3F, and S3A). At the higher dose (10 mg/kg), GNE-0723 reduced the

power across frequency bands and brain states, including delta, theta, alpha, and gamma (Figures 3E, 3F, and S3A). Contrary to GNE-0723, (+)-MK-801 prominently increased the power of low-frequency oscillations, including the delta (0.5–6 Hz) band (Figure S3B). Thus, enhancing GluN2A-containing NMDARs by low doses of GNE-0723 predominantly suppresses low-frequency (12–20 Hz) oscillations without altering gamma oscillations or locomotor activity, whereas blocking NMDAR function predominantly increased low-frequency oscillatory power and induced hyperactivity.

Pathological Network Hypersynchronization Emerges during Low-Frequency Oscillatory Activity in DS and AD Mouse Models

Oscillatory rhythms reflect behavioral states and strongly modulate network synchrony in health and disease (Palop and Mucke, 2016). Resting brain states with increased low-frequency (e.g., 12–20 Hz) oscillatory power are characterized by large-amplitude EEG signals and a high degree of network synchrony between adjacent brain regions (Palop and Mucke, 2016). Because such hypersynchronous brain states are associated with epileptic activity, GluN2A PAM treatment could potentially be beneficial in epileptic brains by reducing low-frequency (12–20 Hz) oscillatory power. Thus, we characterized Scn1a-KI mice that carry a heterozygous loss-of-function knockin (KI) mutation in the voltage-gated sodium channel Scn1a gene (Scn1a-KI mice), which results in Nav1.1 haploinsufficiency and DS (Ogiwara et al., 2007; Yamakawa, 2009), and the J20 mouse model of AD, which overexpresses human amyloid precursor protein with the Swedish and Indiana familial AD mutations (Mucke et al., 2000). Scn1a-KI and J20 mice have interneuron deficits, spontaneous epileptiform discharges (EDs), and cognitive deficits (Martinez-Losa et al., 2018; Ogiwara et al., 2007; Palop et al., 2007; Palop and Mucke, 2016; Verret et al., 2012).

To determine whether pathological network hypersynchronization is associated with oscillatory rhythms in Scn1a-KI and J20 mice, we monitored spontaneous EDs, oscillatory rhythms, and locomotor activity by intracranial EEG recordings while mice explored a novel environment. Consistent with our previous findings (Martinez-Losa et al., 2018), Scn1a-KI and J20 mice had spontaneous EDs (Figure 4A, top), which were much more frequent during periods of low locomotor activity and almost absent during high locomotor activity (Figure 4A, bottom). Oscillatory frequency analyses revealed that the power of gamma-(30–80 Hz) and low-frequency (12–20 Hz) oscillations were strongly anticorrelated and associated with high and low locomotor activity, respectively, in Scn1a-KI and J20 mice (Figures 4A and 4B). Linear regression analysis showed that EDs were indeed strongly associated with increased 12- to 20-Hz power and decreased 30- to 80-Hz power in DS and J20 mice (Figures 4C and 4D). These results indicate that aberrant network hypersynchronization is tightly correlated with oscillatory rhythms and behavioral states in Scn1a-KI and J20 mice.

Enhancing GluN2A-Containing NMDARs Ameliorates Pathological Network Hypersynchrony in Scn1a-KI and J20 Mice

Because increased low-frequency (12–20 Hz) oscillatory power was strongly associated with network hypersynchronization in Scn1a-KI and J20 mice (Figure 4) and in humans with epilepsy (Boly et al., 2017; Vaudano et al., 2017; Matsumoto et al., 2013; Palop and Mucke,

2016), we wondered whether the suppressive effects of GNE-0723 on low-frequency oscillations could ameliorate the network hypersynchronization seen in these mouse models. To test this hypothesis, we recorded two 50-min EEG sessions in Scn1a-KI and J20 mice before (pretreatment session) and 30 min after administration of vehicle or 3 mg/kg GNE-0723, a dose that significantly reduced 12- to 20-Hz power with minimal or no effects on locomotor activity (Figure 3).

As expected, 12- to 20-Hz power increased during the two EEG sessions as mice habituated to the arena and their exploratory activity decreased (Figures 5A and S4A). Scn1a-KI mice showed elevated 12- to 20-Hz power relative to WT controls during the baseline session, reflecting the aberrant network synchrony in this model. GNE-0723 significantly reduced 12- to 20-Hz power for both WT and Scn1a-KI mice relative to vehicle-treated controls (Figures 5A and 5B) without affecting locomotor activity (Figure S4A) or gamma oscillatory power (30–80 Hz; Figure S4B). Because increased 12- to 20-Hz power is associated with EDs in Scn1a-KI mice (Figure 4), we next examined whether the suppressive effects of GNE-0723 on 12- to 20-Hz power were also associated with reduced rates of EDs. Indeed, we found that 3 mg/kg GNE-0723 significantly reduced the frequency of EDs in Scn1a-KI mice when compared to vehicle (Figures 5C–5E), whereas no differences on EDs were observed during the baseline session. Consistent with our initial observations (Figure 4), the power of 12–20 Hz negatively correlated with locomotor activity (Figure 5F) and positively correlated with EDs (Figure 5G) in Scn1a-KI mice, indicating a clear relationship between behavioral state and aberrant network hypersynchrony in this mouse model. Interestingly, GNE-0723 did not alter the tight correlation between 12- to 20-Hz power and ED rate (Figure 5G) but instead reduced 12- to 20-Hz power across locomotor activity levels (Figure 5F). These results indicate that 12- to 20-Hz power and EDs are tightly linked in Scn1a-KI mice and that GNE-0723 may reduce EDs by suppressing pro-hypersynchronous low-frequency oscillations.

Because aberrant network hypersynchronization was also tightly linked to oscillatory activity in J20 mice (Figure 4), we next tested whether GNE-0723 could also reduce the ED phenotype in J20 mice. As observed in Scn1a-KI mice, EDs and 12- to 20-Hz power aberrantly increased during the two EEG sessions as mice decreased their exploratory activity (Figures 6 and S5). GNE-0723 reduced 12- to 20-Hz power in both WT and J20 mice (Figures 6A and 6B) and reduced the rate of EDs in J20 mice (Figures 6C–6E). As expected, 12- to 20-Hz power correlated negatively with locomotor activity (Figure 6F) and positively with ED rate (Figure 6G). As in the Scn1a-KI mice, GNE-0723 reduced both 12- to 20-Hz power and ED rate in J20 mice without altering the relationship between the two (Figure 6G) and without altering locomotor activity (Figure S5A) or gamma oscillatory power (Figure S5B), suggesting that the reduction of 12- to 20-Hz power is upstream of the reduction of EDs. Thus, enhancing GluN2-containing NMDARs with GNE-0723 reduces epileptiform brain activity in two distinct mouse models with EDs.

Chronic GNE-0723 Treatment Ameliorates Memory Impairments in Scn1a-KI and J20 Mice

To determine whether chronic GNE-0723 treatment ameliorates cognitive deficits in J20 and Scn1a-KI mice, we orally treated J20 and Scn1a-KI mice and their respective littermate WT

controls with 3 mg/kg GNE-0723 or vehicle every other day for 5 weeks (Figure S6A). We used this regimen because this dose was effective at modulating oscillatory rhythms and lowering epileptiform discharges in J20 and Scn1a-KI mice, and every other day dosing achieved sustained brain exposure with total GNE-0723 concentrations of ~0.2 μM observed 48 h after the last dose (Figures S6B and S6C).

Cognitive performance was assessed by the Morris water maze (MWM) test in J20 mice. After 2 weeks of treatment, vehicle- and GNE-0723-treated J20 mice showed similar impairments in the hidden platform component of the MWM test as indicated by increased swim distance to reach the platform compared to WT groups (Figure 7A, left). However, an early probe trial 24 h after 3 days of MWM training revealed a significant quadrant preference (reference memory) in GNE-0723-treated J20 mice, but not in vehicle-treated J20 mice (Figure 7B, left), indicating that GNE-0723 enhances memory retention in J20 mice. After 5 days of MWM training, all groups had significant quadrant preference, albeit stronger preference in WT groups (Figure 7B, right). Next, we challenged the mice to locate a smaller hidden platform for 3 extra days of hidden MWM training (Figure 7A, right). Interestingly, under these conditions, all groups showed comparable performance during training and the 24-h probe trial thereafter (Figure 7C, left). However, a late 196-h probe trial revealed that GNE-0723-treated J20 mice and WT groups still remembered the location of the platform and spent more time in the correct target quadrant, whereas vehicle-treated J20 mice exhibited no target preference (Figure 7C, right). Notably, two-way ANOVA showed significant treatment (p = 0.009) and genotype (p = 0.025) effects with no genotype 3 treatment interaction, indicating that GNE-0723 improved memory retention in both WT and J20 mice. Thus, GNE-0723 treatment improved memory retention in J20 mice (Figure 7B, left) and improved long-term memory consolidation in J20 and WT mice (Figure 7C, right). This cognitive benefit in the WT mice suggests that enhanced memory may not necessarily be secondary to reduced epileptiform activity in the J20 mice but may be due to the effects of NMDAR enhancement on oscillatory rhythms.

Cognitive performance in Scn1a-KI mice was assessed in the contextual fear conditioning test, because Scn1a-KI mice did not show robust cognitive deficits in the MWM test (Figures S6D and S6E). Compared to WT controls, vehicle- and GNE-0723-treated Scn1a-KI mice exhibited impaired freezing response (fear learning) to foot shocks during contextual fear conditioning training (Figure 7D). However, GNE-0723-treated Scn1a-KI mice showed improved contextual fear learning compared to vehicle-treated Scn1a-KI mice (Figure 7D, training), suggesting that GNE-0723 enhances fear learning in Scn1a-KI mice. During the 24-h recall test, both vehicle- and GNE-0723-treated Scn1a-KI mice exhibited comparable freezing. However, the 48-h recall test in a similar environment showed that GNE-0723-treated Scn1a-KI mice had improved memory retention compared to vehicle-treated Scn1a-KI mice. Thus, GNE-0723 improved both learning and memory recall in the fear conditioning test. The effects of GNE-0723 on fear memory could not be assessed in J20 mice, because J20 mice did not show robust cognitive deficits in the fear conditioning test (Figure S6F).

DISCUSSION

GluN2A-subunit-containing NMDAR allosteric potentiation had contrary behavioral and brain oscillatory effects to NMDAR blockade *in vivo*, including reduced locomotor activity and broadly decreased EEG oscillatory power. Aberrant increases of low-frequency oscillatory power reflect network hypersynchronization (Boly et al., 2017; Vaudano et al., 2017; Matsumoto et al., 2013) and may contribute to the pathophysiology of DS and AD (Palop and Mucke, 2016). Consistently, low doses of GNE-0723 reduced aberrantly increased low-frequency (12–20 Hz) oscillatory power, ameliorated epileptiform activity, and improved cognitive functions in mouse models of DS and AD. Thus, GluN2A PAMs could represent a potential therapeutic strategy for normalizing pathological network activity and cognitive functions in diseases with network hypersynchrony, such as epilepsy and AD. Interestingly, GNE-0723 treatment also modulated low-frequency oscillations and improved memory retention in wild-type mice, indicating that the pro-cognitive effects of GNE-0723 do not necessarily depend on its antiepileptic properties.

Potential Mechanisms of NMDAR Modulator Effects on Brain Rhythms

The behavioral effects of NMDAR blockade in rodents, such as hyperactivity and stereotypies, are well established and have been used to model the positive symptoms of schizophrenia (Adell et al., 2012). NMDAR antagonists increase the power of both low- and high-frequency oscillations (Lazarewicz et al., 2010), indicative of hypersynchronous oscillatory rhythms. The cellular effects of (+)-MK-801 treatment, including reduced fast-spiking interneuron activity (Homayoun and Moghaddam, 2007) and increased expression of activity-dependent immediate early genes in pyramidal neurons (Gao et al., 1998; Hughes et al., 1993), suggest that suppressed inhibitory interneuron firing and increased excitatory neural activity may underlie the network effects, which manifest as increased locomotor activity and increased EEG power.

In contrast, *in vivo* effects of GNE-0723 involve reduced low-frequency (12–20 Hz) oscillatory power, a frequency band associated with brain resting state and network hypersynchrony in DS and AD models (Figure 4). Thus, GNE-0723 treatment seems to modulate brain state, favoring active states and desynchronized neuronal activity. Recordings from acute brain slices show that GNE-0723 can enhance NMDAR currents in both pyramidal cells and PV interneurons (Figure 2), suggesting that both cell types contribute to *in vivo* effects of GNE-0723. However, the relative effects of GNE-0723 on excitatory and inhibitory neurons *in vivo* will ultimately depend on the level of GluN2A-containing NMDAR activation in each neuron type and its downstream functional effects. As with NMDAR antagonists, it is tempting to speculate that the effects of GluN2A-containing NMDAR activation on circuit function *in vivo* may have a predominant effect on inhibitory interneurons, because these cells are more depolarized and fire action potentials at high rates, providing ongoing depolarization, removal of Mg^{2+} block, and basal NMDAR activity (Cohen et al., 2015; Homayoun and Moghaddam, 2007). Supporting this notion, GNE-0723 suppressed locomotor and rearing activity in a GluN2A- and dose-dependent manner, consistent with enhanced inhibition and general sedation, and reduced low-frequency oscillatory power observed in WT mice (Figure 3), an effect similar to $GABA_A$

PAMs, such as the benzodiazepine lorazepam (Saletu et al., 2006). However, GNE-0723 does not cause the paradoxical increase in EEG power above 15 Hz that is a hallmark of benzodiazepines (van Lier et al., 2004), suggesting that the therapeutic profile of an GluN2A PAMs is likely to be different from benzodiazepines.

Consistent with restoration of interneuron-dependent network functions, GNE-0723 treatment rescued excessive low-frequency oscillatory power and epileptiform activity in the DS mouse model (Figure 5). Nav1.1 is predominately expressed by inhibitory interneurons, including PV and somatostatin interneurons, and impaired inhibitory function has been proposed as a major pathogenetic mechanism in DS (Catterall et al., 2010; Ogiwara et al., 2007; Rubinstein et al., 2015; Tai et al., 2014; Yamakawa, 2009; Yu et al., 2006). The J20 mouse model of AD also features reduced Nav1.1 expression levels and network hypersynchrony. Restoring interneuron function by Nav1.1-BAC expression, Nav1.1-overexpressing interneuron transplants or treatment with the anticonvulsant drug levetiracetam can reduce the pathological EEG spikes in these mice (Martinez-Losa et al., 2018; Sanchez et al., 2012; Verret et al., 2012). As with the DS model mice, GNE-0723 also reduced epileptiform activity in the J20 AD model mice (Figure 6), confirming a benefit of the GluN2A PAM in two separate models of network hypersynchrony and impaired interneuron function. In both models, we observed a strong relationship between oscillatory power and EDs, with EDs occurring more often during periods of reduced high-frequency and elevated low-frequency oscillatory power (Figure 4), which is consistent with intracranial EEG measurements in epilepsy patients (Matsumoto et al., 2013). The predominant effect of 3 mg/kg GNE-0723 in both disease models (and controls) was to significantly reduce low-frequency oscillatory power and to reduce the rate of EDs. Interestingly, GNE-0723 treatment did not affect the relationship between low-frequency oscillatory power and ED rate in either model, suggesting that the reduction in low-frequency oscillatory power could be sufficient to drive the suppression of epileptiform activity.

Potential Mechanisms of NMDAR Modulator Effects on Memory Retention

Prolonged reduction of network hypersynchrony in J20 and Scn1a-KI mice can provide cognitive benefit (Gheyara et al., 2014; Han et al., 2012; Martinez-Losa et al., 2018; Sanchez et al., 2012; Verret et al., 2012). We hypothesized that chronic GNE-0723 treatment would also be beneficial for cognitive functions because it had antiepileptic properties. During ongoing GNE-0723 treatment, we observed improved reference memory in treated J20 mice in an early probe trial after 3 days of water maze training. Remarkably, we also observed increased memory retention in both J20 and NTG mice when tested 8 days after training. The improved memory retention in WT mice suggests potentiating GluN2A-subunit-containing NMDARs can have beneficial effects on memory even outside of the context of impairments driven by pathological network hypersynchrony. Because GNE-0723 reduces low-frequency oscillatory activity, which is associated with resting brain states and increased synchrony, we speculate that the pro-cognitive effects of GNE-0723 might also be mediated by promoting brain rhythms that favor active brain states. Consistent with the J20 behavioral data, we also observed enhanced memory formation in treated Scn1a-KI mice during the

training session of the fear conditioning test and enhanced memory retention during the 48 h recall test.

Although we have provided speculation on plausible roles of enhancement of synaptic NMDARs in pyramidal neurons and/or interneurons that could contribute to *in vivo* GluN2A PAM effects, it is also important to keep in mind the numerous sites of action that NMDAR PAMs could have *in vivo*. For example, GluN2A NMDARs are expressed in diverse neuron types throughout the various circuits of the brain and modulation of tonic or synaptic NMDAR currents or even presynaptic or astrocyte NMDARs could conceivably occur during *in vivo* treatment. It is also important to note that the majority of NMDARs in native brain tissue are likely various triheteromeric assemblies, for example, composed of two GluN1 subunits and GluN2A/GluN2D subunits (interneurons) or GluN2A/GluN2B subunits (interneurons and pyramidal cells), which are likely potentiated by GNE-0723 with varying potency. Thus, additional studies will be needed to identify the GluN2A-subunit-containing NMDAR assemblies, the cell types, and the circuits responsible for the cognitive benefits driven by activation of GluN2A subunit-containing NMDARs *in vivo*.

Therapeutic Potential of NMDAR PAMs

Although the results with DS and AD mouse models suggest therapeutic promise of GluN2A PAMs, challenges remain for realizing this type of approach. A concern with glutamate receptor PAMs, including NMDAR PAMs, is that, in addition to beneficial effects at lower doses, there is the potential for neuronal over-excitation and triggering of seizures at higher doses, as is seen with AMPAR and mGluR PAMs (Shaffer et al., 2013; Yang et al., 2016). With this concern in mind, we have limited dosing of GNE-0723 to the lower dose (3 mg/kg) in order to focus on effects on physiological function, while avoiding potential adverse effects at higher doses.

Although NMDAR potentiation can be achieved in different ways (e.g., enhancing peak current or slowing deactivation; Hackos and Hanson, 2017), we do not currently have compounds with different modes of potentiation that can be compared *in vivo*, and it remains unclear which *in vitro* properties of GNE-0723 are important for the *in vivo* effects. Thus, future development of *in vivo* GluN2A PAM tools with contrasting modes of action could provide further insight into the potential impacts of NMDAR enhancement on circuit function. Various mutations in *GRIN2A*, the gene encoding GluN2A, have been identified in syndromic causes of childhood epilepsy, including both loss of function and gain of function (Addis et al., 2017; Carvill et al., 2013; Gao et al., 2017; Lemke et al., 2013; Lesca et al., 2013; Serraz et al., 2016; Yuan et al., 2014), suggesting complex relationships between GluN2A-containing NMDAR function and network excitability during development. Interestingly, a recent study showed that a compound closely related to GNE-0723 could rescue loss-of-function phenotypes seen in NMDAR currents measured from cells expressing NMDARs with epilepsy patient *GRIN2A* mutations (Addis et al., 2017).

Finally, although we originally pursued GluN2A-selective PAMs based on theoretical concerns over potential excitotoxicity with overactivation of GluN2B NMDARs (Hardingham et al., 2002; Hu et al., 2009; Li et al., 2011), it has not been definitively established that GluN2B overactivation actually plays a detrimental role in the context of

AD (Hanson et al., 2014; Texidó et al., 2011). Thus, it remains possible that other PAMs without GluN2A selectivity could also show efficacy in AD mouse models.

Overall, GNE-0723 represents a useful tool compound that reveals the *in vivo* consequences of pharmacological enhancement of GluN2A-containing NMDARs. The profile of effects suggests GluN2A PAMs can act to normalize hyperactive brain networks and can enhance memory retention in DS and AD mouse models. Future studies using this tool compound and building on these results should reveal new insight into the physiological roles of NMDARs in different cell types and circuits. Following the initiation of *in vivo* work with GNE-0723 reported here, we have also discovered another GluN2A PAM, GNE-5729, which potentiates NMDAR currents in a similar manner as GNE-0723 and exhibits even better pharmacokinetic properties, which should be useful for future *in vivo* studies (Villemure et al., 2016). The findings of the present study indicate that NMDAR PAMs could have therapeutic potential not only in disorders like schizophrenia, where the pathophysiology is thought to involve NMDAR hypofunction, but more broadly in diseases where network hyperexcitability may contribute to pathology or symptoms, including DS, other forms of epilepsy, and AD.

STAR★METHODS

LEAD CONTACT AND MATERIALS AVAILABILITY

Further information and requests for resources and reagents should be directed to and will be fulfilled by the Lead Contact, Jesse Hanson (hanson.jesse@gene.com). This study did not generate new unique reagents.

EXPERIMENTAL MODEL AND SUBJECT DETAILS

Mice were housed at AAALAC-approved facilities. Animal studies were approved by the Institutional Animal Care and Use Committees and were conducted in accordance with the NIH Guide for the Care and Use of Laboratory Animals. Food and water were available *ad libitum*. Pharmacokinetic studies (Figure 1) were performed using male C57BL/6 mice from Charles River Laboratories (Hollister, CA, USA). Brain slice electrophysiology experiments (Figure 2) used PV-cre mice crossed to tdTomato reporter mice on the C57BL/6J background (Tanahira et al., 2009). Locomotor studies with GNE-0723 (Figure 3) used GluN2A^{KO} and WT littermate mice on the C57BL/6J background (Kadotani et al., 1996). Locomotor studies with MK-801 (Figure S2) and EEG brain state studies (Figure 3) used C57BL/6J mice from The Jackson Laboratory (Sacramento, CA, USA). EEG and behavioral studies (Figures 4, 5, 6, and 7) used Scn1a-KI and littermate control mice on a C57BL/6J background (Ogiwara et al., 2007) and J20 and littermate control mice on a 50% C57BL/6J and 50% FVB/N background (Verret et al., 2012). Unless indicated otherwise, EEG and behavioral measurements were done in sex-mixed groups in adult mice using automated recording systems by investigators who were unaware of the genotype or treatment of the mice. The age of mice is indicated in the figure legends.

METHOD DETAILS

Dosing—Doses of GNE-0723 were administered via oral gavage as 0.5% methylcellulose and 0.2% Tween 80 (MCT) suspension. Vehicle was used as control. Drug doses for GNE-0723 are expressed as mg/kg of free base. (+)-MK-801 and (−)-MK-801 were dissolved in saline and administered IP; doses are expressed as mg/kg of the maleate salt. Application volume was 5–10 mL/kg.

Pharmacokinetics—After PO dose administration, blood and brain samples were collected from mice at the indicated times post-dose. Blood samples were collected into K_2EDTA Microtainer tubes (Becton Dickinson; Franklin Lakes, NJ, USA) and were centrifuged at a relative centrifugal force (RCF) of $2,800 \times g$ for 5 minutes. Plasma was decanted and stored at −80°C until thawed for analysis. The concentrations of GNE-0723 in plasma and brain samples were determined by liquid chromatography–tandem mass spectrometry (LC-MS/MS) assay using indomethacin as an internal standard (IS). The unbound fractions in plasma and brain homogenate of GNE-0723 were determined in a 48-well rapid equilibrium dialysis (RED) device using a dialysis membrane with a molecular weight cut-off value of 8,000 Da (Pierce Biotechnology, Rockford, IL, USA). The unbound fraction in plasma and unbound fraction in the brain homogenate were calculated as a ratio of buffer concentration to plasma or brain concentration, and these values were used to determine the unbound plasma and brain concentrations in the samples.

Cell-line rapid solution exchange electrophysiology—Whole-cell patch-clamp recordings from CHO cell lines with doxycycline-inducible (Dox) GluN1/GluN2A were performed using the Dynaflow Resolve rapid solution exchange system (Cellectricon, Mölndal, Sweden) as previously described (Hackos et al., 2016). Except where otherwise indicated experiments were performed at RT. For the set of experiments performed at 37°C, a DFT100201 Temperature Controller Unit and DFT100202 Heat Stage were added to the Dynaflow system (Cellectricon). Intracellular solution contained (in mM): 140 CsF, 10 NaCl, 1.5 MgCl2, 5 EGTA, 10 HEPES, adjusted to pH 7.2 with CsOH. The extracellular recording solution contained (in mM): 150 NaCl, 3 KCl, 1 CaCl2, 5 glucose, 10 HEPES, adjusted to pH 7.4 with NaOH.

Cell-line synaptic-like glutamate application—Whole-cell patch-clamp recordings were made from CHO cell lines as above and 100 μM Glu was applied for a 5ms pulse duration using a 2-barrel theta tube perfusion system with a P-601.30L PiezoMove linear actuator (PI, USA).

Brain slice electrophysiology—Mice were anesthetized using isoflurane prior to decapitation and 300-mm-thick coronal slices were prepared with a vibrating sectioning system (Leica, Germany). Whole-cell recordings were made from layer 5 pyramidal neurons or PV-positive interneurons in coronal cortical slices using 2–3-month-old PV-cre × tdTomato mice. Recordings were made at RT in oxygenated artificial cerebrospinal fluid (ACSF) containing (in mM) 127 NaCl, 2.5 KCl, 1.3 MgSO4, 2.5 CaCl2, 1.25 Na2HPO, 25 NaHCO3, 25 glucose. Slices were prepared in ice-cold oxygenated ACSF with the MgSO4 concentration elevated to 7 mM, NaCl replaced with 110 mM choline, and with 11.6 mM

Na-ascorbate and 3.1 mM Na-pyruvate. Slices recovered in this same solution at 34 C for 30 min before being transferred to regular ACSF at RT for storage for at least 1 hour prior to recording. tdTomato fluorescence was visualized using a Zeiss Axio Examiner.Z1 microscope. For current-clamp recordings, intracellular solution consisted of (in mM) 120 K-gluconate, 20 KCl, 0.5 EGTA, 10 HEPES, 2.5 MgCl2, 4 Na2ATP, 0.3 NA3GTP and 10 phosphocreatine. For voltage clamp experiments, the K-gluconate was replaced with Cs-methanesulfonate; KCl was replaced with CsCl; and 5 mM QX-314 Cl was added. NMDAR EPSCs were measured in response to electrical stimulation (0.2 ms pulse duration in constant current mode with intensity adjusted to elicit a baseline EPSC in the 25–100 pA range) 100–200 mm away from the recorded cell at 30 s inter-stimulus intervals, and were recorded at a holding potential of −70 mV in the presence of reduced Mg2+ (0.5 mM). Signals were low pass filtered at 10 kHz. NMDAR EPSCs were isolated using 10 μM NBQX disodium salt and 100 μM PTX. 100 μM AP5 applied at the end of the recording confirmed isolation of pure NMDAR EPSCs. Series resistance was monitored and recordings were discarded if series resistance changed by more than 15% or if apparent loss of voltage clamp control occurred as reflected by a sudden change in the EPSC waveform. NMDAR EPSC peak current amplitude, current area, and decay time constants were measured using Clampfit and average values during the last 5 minutes of the experiment are reported as a percentage of the baseline value.

Intracranial EEG comparison of GNE-0723 and MK-801 in WT mice

Intracranial EEG surgery: Male mice (2–3 months old) were anesthetized with isoflurane (~3.5% at 700 mL/min) and given a subcutaneous injection of 4 mg/kg of Carprofen (Henry Schein, Dublin, OH, USA). A prefabricated EEG/EMG headmount (model #8201 Pinnacle Technologies, Lawrence KS, USA) was secured to the skull with two 0.10" screws anterior (#8209, Pinnacle Technologies) and two 0.12" screws posterior (#8212, Pinnacle Technologies) implanted at the following stereotactic coordinates relative to bregma (lateral, anterior in mm): reference electrode −1.2, −2.5 (left visual cortex); ground electrode −1.2, 3 (left frontal cortex); recording electrode: 1.2, 3 (right frontal cortex). Silver epoxy (#8226, ResinLab, Germantown WI, USA) was then applied to the screws to ensure electrical conduction, and the entire assembly was secured to the skull with VetBond (#1469SB 3M, Saint Paul MI, USA) and dental acrylic (#1230, Lang Dental Manufacturing, Wheeling IL, USA). The EMG electrodes were inserted into small pockets in the nuchal muscle.

Synchronized Video

EEG, and EMG recordings: Mice were recorded on two consecutive days during the middle of the light cycle. Each recording session lasted 150 minutes. Mice were dosed with vehicle immediately before recording on day 1 and with vehicle or compound on day 2. The first 20 minutes of each recording were excluded from further analysis to allow time for the drug to reach maximal brain exposure. Recordings occurred in four 25.4 cm diameter cylindrical acrylic arenas with bedding using 4-channel video/tethered-EEG systems (Pinnacle Technologies). EEG/EMG data were sampled with 16 bit resolution at 500 Hz, and band-pass filtered between 0.5 and 125 Hz for EEG and 10 to 125 Hz for EMG. 320×240 pixel grayscale videos were captured at 10 fps.

Video EEG/EMG analysis: EEG/EMG data were exported to European Data Format (.edf) files for analysis in MATLAB 2014a (Mathworks, Natick, MA, USA). Spectrograms were calculated by the multitaper method with three tapers, 1 s windows, 0.1 s steps, and 2 Hz bandwidths using the Chronux toolbox (http://chronux.org) (Mitra and Bokil, 2008). The spectrograms were averaged into 5 s epochs for sleep state classification using a 3-step semi-automated hierarchical algorithm based on the EMG and EEG channel 2 signals (Louis et al., 2004). Briefly, the step 1 threshold was manually chosen to best separate the EMG_{RMS} signal (above threshold = Active Wake, below threshold = next step), the step 2 threshold separated $(\delta*\alpha)/(\beta*\gamma)$ (above = NREM, below = next step), and the step 3 threshold separated $(\theta^2)/(\delta*\alpha)$ (above = REM, below = Quiet Wake). The frequency bands for sleep scoring were defined as: delta (δ) = 0.5 to 6 Hz, theta (θ) = 6 to 10 Hz, alpha (α) = 10.5 to 15 Hz, beta (β) = 22 to 30 Hz, and gamma (γ) = 35 to 56 and 64 to 100 Hz to avoid potential 60 Hz noise. We defined γ = 30 to 80 Hz for calculating the scatterplots in Figures 3E and 3F to maintain consistency with the EEG experiments in the Scn1a-KI and J20 mice. For Figures 3E, 3F, and S3 the average day 2 (drug) EEG power for each mouse was normalized by the day 1 (vehicle) power for that mouse, and by the average change in EEG power from day 1 to day 2 for the vehicle-dosed mice. These normalizations allowed the drug effects to be isolated from changes in EEG power due to habituation to the arena across days.

Scn1a-KI and J20 EEG recordings on freely moving mice—Sex-mixed 9–13-month-old Scn1a-KI and 7 – 11-month-old mice were implanted and recorded for video EEG monitoring as (Martinez-Losa et al., 2018; Verret et al., 2012). Cortical EEG recordings were performed on freely moving mice in an open-field chamber ($40 \times 40 \times 30$ cm; automated Flex-Field/Open Field Photobeam Activity System; San Diego Instruments, San Diego, CA, USA) using the EEG Harmonie software (version 5.0b, Stellate, Natus Neurology, Middleton, VA, USA). A crossover design was used for the drug treatment studies. We first recorded a 50-min EEG pretreatment session on day 1 followed by a second 50-min EEG treatment session on day 3, in which mice orally received vehicle or 3 mg/kg GNE-0723 treatments 30 minutes before the recording session started. Mice were kept in regular mouse cages between recording sessions, including the 30-min period after dosing. After a washout period of > 3 weeks, we repeated the same experimental design but mice received the alternative treatment (crossover design). The number of epileptiform discharges (EDs) was automatically detected with a Gotman spike detector (threshold 6; Harmonie, Stellate). For spectral analyses, 50-min segments of unfiltered EEG recordings (sampling rate 200 Hz) from freely moving mice were analyzed using LabChart 7 Pro software (AD Instruments, Colorado Springs, CO, USA). The 12–20-Hz (α–β) and 30–80-Hz (γ) bands were used to calculate the low- and high-frequency oscillatory power, respectively. Fast Fourier transform (FFT) was applied with a Hann cosine-bell window with 50% overlap between windows of 500-ms epochs and a 512 point FFT size to obtain a resolution of 0.39 Hz. The low- and high-frequency oscillatory power values for each 500-ms epoch were further averaged over 60 s of EEG recording, using the median values, to remove potential noise. Because high- (30–80 Hz) and low- (12–20 Hz) frequency oscillatory power were associated with high and low behavioral activity respectively (Figure 4), we normalized low-frequency (12–20 Hz) oscillatory power to resting periods and high-frequency (30–80 Hz) power to active periods for each mouse, which represent the behavioral states with the

lowest oscillatory power for each frequency band. To calculate relative 30–80 Hz power, the *y*-intercept at 0 movements/min was calculated for each mouse by linear regression analysis using the 50-min data points of movement frequency (x; beam breaks/min) and the absolute 30–80 Hz power (y; V^2) for the pretreatment session. The *y*-intercept of the absolute 30–80 Hz power value for the pretreatment EEG session was used to normalize the 100 min of EEG data points of pretreatment and treatment sessions within each mouse. Thus, 1.0 indicates the high-frequency (30–80) Hz power at resting during the pretreatment session. To calculate relative 12–20 Hz power, the average of the absolute 12–20 Hz power (V^2) during periods of intermediate locomotor activity (20–100 beam breaks/min) was used to normalize the 100 min of EEG data points of 12–20 Hz power within each mouse. Thus, 1.0 indicates the 12–20 Hz power during active periods in the pretreatment session. Finally, normalized signals from both hemibrains were averaged to obtain the power values for each mouse.

Behavioral testing

Open field test: Sex-mixed 3–6-month-old (GNE-0723 experiments in GluN2A[KO] and WT littermates, Figure 3) and 2–3-month-old male mice (MK-801 experiments, Figure S2) were maintained on a 14/10 hour light/dark cycle and tested during the light phase. PAS™ open-field recording systems (San Diego Instruments, San Diego, CA, USA) consisted of transparent thermoplastic cages (40.5 (W) × 40.5 (L) × 38 (H) cm) surrounded by a locomotor frame and a rearing frame fitted with infra-red beams to automatically record horizontal locomotor activity (3 cm above floor) and rearing activity (7.5 cm above floor), respectively. The total number of beam breaks for both ambulatory locomotor activity and rearing were obtained for bin sizes of 10 min and reported as ambulatory beam breaks and rearings per minute, respectively. Locomotor analyses are based on aggregated data from a 30-min time window beginning 30 min after dosing. This time window corresponds to the 40–60 min bins for GNE-0723 and 70–90 min bins for MK-801. Data were analyzed using one-way, between-subjects ANOVA. Post hoc comparisons were made using Tukey's HSD in order to account for more than two comparisons between factors or factor levels. Analyses and graphs were generated using JMP 10.02 (SAS Institute, Cary, NC, USA). Four GluN2A KO mice that had seizures during weighing prior to dosing were excluded from locomotor analyses.

Morris water maze test: Cognitive function of sex-mixed 4–6-month-old J20 (Figure 7), 10–12-month-old Scn1a-KI (Figure S6) and littermate control mice was assessed using the Morris water maze test. The pool is 122 cm in diameter containing opaque white water. The standard platform is 14×14 cm and the small platform is 10×10 cm. Mice were trained to locate a hidden platform based on spatial cues on surrounding walls. Each training day consists of 2 sessions 4 hours apart, each session is 2 trials 20–30min apart. As indicated, mice were trained for 5 (J20 mice) or 6 (Scn1a-KI mice) days with the standard platform. J20 mice received additional 3 days of hidden training with a small platform. The location of the hidden platform remained constant and the drop points of the mice were semi-randomly assigned. As indicated, one minute 24-hour probe trials were performed after 3 days and after the conclusion of the hidden platform training with the standard and small platforms. J20 mice received an additional one 192-hour probe trial after the hidden training. Activity of the mice were monitored using an EthoVision video tracking system (Noldus Information

Technology). Swim distance and latencies to reach the hidden platform were used to measure performance in training trials. Swim speed was not altered by chronic GNE-0723 treatment (WT-Vehicle = 18.5 ± 0.4, J20-Vehicle = 19.6 ± 0.4, WT-GEN-0723 = 18.1 ± 0.5, J20-GEN-0723 = 18.9 ± 0.5; mean (cm/s) ± SEM). Percentage (%) time spent in the hidden platform target quadrant versus average % time spent in the other 3 quadrants were used to assess reference memory. Mice were single-housed for the duration of this test.

Contextual fear conditioning test: Cognitive function of sex-mixed 10–12-month-old Scn1a-KI (Figure 7), 4–6-month-old J20 (Figure S6) and littermate control mice was assessed using the contextual fear conditioning test. The test used 4 identical computer-controlled chambers ($28 \times 21 \times 22$ cm) with 18 stainless steel floor rods connected to a shock scrambler and generator (4 mm diameter, 1.5cm apart) (Med Associates). On day one, mice were habituated in the chambers for 5min to record baseline freezing behavior, then mice were given four 1 s shocks (0.45mA) 2 min apart. For the 24-hour and 48-hour contextual recall tests, mice were placed in the same chambers for 5 min with identical (24-hour recall) or similar (48-hour recall) configurations. Freezing behavior was automatically recorded by a video-tracking system and defined as the absence of any visible movement except respiration (motion threshold = 18, detection method = linear; Med Associates). Total activity during baseline was not altered by chronic GNE-0723 treatment (WT-Vehicle = 155 ± 8, J20-Vehicle = 194 ± 11, WT-GEN-0723 = 162 ± 14, J20-GEN-0723 = 177 ± 10; mean (average motion index) ± SEM). The chambers were cleaned with 70% ethanol after each mouse.

QUANTIFICATION AND STATISTICAL ANALYSIS

Statistical analyses were done with STATA, Prism, or JMP. Graphs were generated with Prism or JMP. As indicated in the figure legends, differences among multiple means were assessed by one-way or two-way ANOVA and Bonferroni, Tukey, or Sidak's post hoc tests. The p values are indicated in the figure panels with the following significance levels, $*p < 0.05$, $**p < 0.01$, and $***p < 0.001$ with two-tailed distribution tests. Null hypotheses were rejected at the 0.05 level.

Number (n) of mice or cells for all statistical analyses is indicated in each graph or in the legend. Unless indicated otherwise, values in figures and text are expressed as mean ± SEM. Statistical tests are indicated in the figure legends.

DATA AND CODE AVAILABILITY

This study did not generate datasets or code.

Supplementary Material

Refer to Web version on PubMed Central for supplementary material.

ACKNOWLEDGMENTS

REFERENCES

Addis L, Virdee JK, Vidler LR, Collier DA, Pal DK, and Ursu D (2017). Epilepsy-associated GRIN2A mutations reduce NMDA receptor trafficking and agonist potency - molecular profiling and functional rescue. Sci. Rep 7, 66. [PubMed: 28242877]

Adell A, Jiménez-Sánchez L, López-Gil X, and Romón T (2012). Is the acute NMDA receptor hypofunction a valid model of schizophrenia? Schizophr. Bull 38, 9–14. [PubMed: 21965469]

Boly M, Jones B, Findlay G, Plumley E, Mensen A, Hermann B, Tononi G, and Maganti R (2017). Altered sleep homeostasis correlates with cognitive impairment in patients with focal epilepsy. Brain 140, 1026–1040. [PubMed: 28334879]

Boyce-Rustay JM, and Holmes A (2006). Genetic inactivation of the NMDA receptor NR2A subunit has anxiolytic- and antidepressant-like effects in mice. Neuropsychopharmacology 31, 2405–2414. [PubMed: 16482087]

Carvill GL, Regan BM, Yendle SC, O'Roak BJ, Lozovaya N, Bruneau N, Burnashev N, Khan A, Cook J, Geraghty E, et al. (2013). GRIN2A mutations cause epilepsy-aphasia spectrum disorders. Nat. Genet 45, 1073–1076. [PubMed: 23933818]

Catterall WA, Kalume F, and Oakley JC (2010). NaV1.1 channels and epilepsy. J. Physiol 588, 1849–1859. [PubMed: 20194124]

Cohen SM, Tsien RW, Goff DC, and Halassa MM (2015). The impact of NMDA receptor hypofunction on GABAergic neurons in the pathophysiology of schizophrenia. Schizophr. Res 167, 98–107. [PubMed: 25583246]

Corbett BF, Leiser SC, Ling HP, Nagy R, Breysse N, Zhang X, Hazra A, Brown JT, Randall AD, Wood A, et al. (2013). Sodium channel cleavage is associated with aberrant neuronal activity and cognitive deficits in a mouse model of Alzheimer's disease. J. Neurosci 33, 7020–7026. [PubMed: 23595759]

Dravid SM, Erreger K, Yuan H, Nicholson K, Le P, Lyuboslavsky P, Al-monte A, Murray E, Mosely C, Barber J, et al. (2007). Subunit-specific mechanisms and proton sensitivity of NMDA receptor channel block. J. Physiol 581, 107–128. [PubMed: 17303642]

Gao XM, Hashimoto T, and Tamminga CA (1998). Phencyclidine (PCP) and dizocilpine (MK801) exert time-dependent effects on the expression of immediate early genes in rat brain. Synapse 29, 14–28. [PubMed: 9552172]

Gao K, Tankovic A, Zhang Y, Kusumoto H, Zhang J, Chen W, Xiang-Wei W, Shaulsky GH, Hu C, Traynelis SF, et al. (2017). A de novo loss-of-function GRIN2A mutation associated with childhood focal epilepsy and acquired epileptic aphasia. PLoS ONE 12, e0170818. [PubMed: 28182669]

Gheyara AL, Ponnusamy R, Djukic B, Craft RJ, Ho K, Guo W, Finucane MM, Sanchez PE, and Mucke L (2014). Tau reduction prevents disease in a mouse model of Dravet syndrome. Ann. Neurol 76, 443–456. [PubMed: 25042160]

Gonzalez-Burgos G, and Lewis DA (2012). NMDA receptor hypofunction, parvalbumin-positive neurons, and cortical gamma oscillations in schizophrenia. Schizophr. Bull 38, 950–957. [PubMed: 22355184]

Hackos DH, and Hanson JE (2017). Diverse modes of NMDA receptor positive allosteric modulation: mechanisms and consequences. Neuropharmacology 112, 34–45. [PubMed: 27484578]

Hackos DH, Lupardus PJ, Grand T, Chen Y, Wang TM, Reynen P, Gustafson A, Wallweber HJ, Volgraf M, Sellers BD, et al. (2016). Positive allosteric modulators of GluN2A-containing NMDARs with distinct modes of action and impacts on circuit function. Neuron 89, 983–999. [PubMed: 26875626]

Hamm V, Héraud C, Bott J-B, Herbeaux K, Strittmatter C, Mathis C, and Goutagny R (2017). Differential contribution of APP metabolites to early cognitive deficits in a TgCRND8 mouse model of Alzheimer's disease. Sci. Adv 3, e1601068. [PubMed: 28275722]

Han S, Tai C, Westenbroek RE, Yu FH, Cheah CS, Potter GB, Rubenstein JL, Scheuer T, de la Iglesia HO, and Catterall WA (2012). Autistic-like behaviour in Scn1a+/− mice and rescue by enhanced GABA-mediated neurotransmission. Nature 489, 385–390. [PubMed: 22914087]

Hanson JE, Meilandt WJ, Gogineni A, Reynen P, Herrington J, Weimer RM, Scearce-Levie K, and Zhou Q (2014). Chronic GluN2B antagonism disrupts behavior in wild-type mice without protecting against synapse loss or memory impairment in Alzheimer's disease mouse models. J. Neurosci 34, 8277–8288. [PubMed: 24920631]

Hardingham GE, Fukunaga Y, and Bading H (2002). Extrasynaptic NMDARs oppose synaptic NMDARs by triggering CREB shut-off and cell death pathways. Nat. Neurosci 5, 405–414. [PubMed: 11953750]

Homayoun H, and Moghaddam B (2007). NMDA receptor hypofunction produces opposite effects on prefrontal cortex interneurons and pyramidal neurons. J. Neurosci 27, 11496–11500. [PubMed: 17959792]

Hu NW, Klyubin I, Anwyl R, and Rowan MJ (2009). GluN2B subunit-containing NMDA receptor antagonists prevent Abeta-mediated synaptic plasticity disruption in vivo. Proc. Natl. Acad. Sci. USA 106, 20504–20509. [PubMed: 19918059]

Hu T, Xiao Z, Mao R, Chen B, Lu MN, Tong J, Mei R, Li SS, Xiao ZC, Zhang LF, and Xiyang YB (2017). Navb2 knockdown improves cognition in APP/PS1 mice by partially inhibiting seizures and APP amyloid processing. Oncotarget 8, 99284–99295. [PubMed: 29245901]

Hughes P, Dragunow M, Beilharz E, Lawlor P, and Gluckman P (1993). MK801 induces immediate-early gene proteins and BDNF mRNA in rat cerebrocortical neurones. Neuroreport 4, 183–186. [PubMed: 8453057]

Javitt DC, and Zukin SR (1991). Recent advances in the phencyclidine model of schizophrenia. Am. J. Psychiatry 148, 1301–1308. [PubMed: 1654746]

Kadotani H, Hirano T, Masugi M, Nakamura K, Nakao K, Katsuki M, and Nakanishi S (1996). Motor discoordination results from combined gene disruption of the NMDA receptor NR2A and NR2C subunits, but not from single disruption of the NR2A or NR2C subunit. J. Neurosci 16, 7859–7867. [PubMed: 8987814]

Kehoe LA, Bernardinelli Y, and Muller D (2013). GluN3A: an NMDA receptor subunit with exquisite properties and functions. Neural Plast. 2013, 145387. [PubMed: 24386575]

Kim DY, Carey BW, Wang H, Ingano LA, Binshtok AM, Wertz MH, Pettingell WH, He P, Lee VM, Woolf CJ, and Kovacs DM (2007). BACE1 regulates voltage-gated sodium channels and neuronal activity. Nat. Cell Biol. 9, 755–764. [PubMed: 17576410]

Kotermanski SE, and Johnson JW (2009). Mg2+ imparts NMDA receptor subtype selectivity to the Alzheimer's drug memantine. J. Neurosci 29, 2774–2779. [PubMed: 19261873]

Krystal JH, Karper LP, Seibyl JP, Freeman GK, Delaney R, Bremner JD, Heninger GR, Bowers MB Jr., and Charney DS (1994). Subanesthetic effects of the noncompetitive NMDA antagonist, ketamine, in humans. Psychotomimetic, perceptual, cognitive, and neuroendocrine responses. Arch. Gen. Psychiatry 51, 199–214. [PubMed: 8122957]

Lazarewicz MT, Ehrlichman RS, Maxwell CR, Gandal MJ, Finkel LH, and Siegel SJ (2010). Ketamine modulates theta and gamma oscillations. J. Cogn. Neurosci 22, 1452–1464. [PubMed: 19583475]

Lemke JR, Lal D, Reinthaler EM, Steiner I, Nothnagel M, Alber M, Geider K, Laube B, Schwake M, Finsterwalder K, et al. (2013). Mutations in GRIN2A cause idiopathic focal epilepsy with rolandic spikes. Nat. Genet 45, 1067–1072. [PubMed: 23933819]

Lesca G, Rudolf G, Bruneau N, Lozovaya N, Labalme A, Boutry-Kryza N, Salmi M, Tsintsadze T, Addis L, Motte J, et al. (2013). GRIN2A mutations in acquired epileptic aphasia and related childhood focal epilepsies and encephalopathies with speech and language dysfunction. Nat. Genet 45, 1061–1066. [PubMed: 23933820]

Li S, Jin M, Koeglsperger T, Shepardson NE, Shankar GM, and Selkoe DJ (2011). Soluble Ab oligomers inhibit long-term potentiation through a mechanism involving excessive activation of extrasynaptic NR2B-containing NMDA receptors. J. Neurosci 31, 6627–6638. [PubMed: 21543591]

Lipton SA (2005). The molecular basis of memantine action in Alzheimer's disease and other neurologic disorders: low-affinity, uncompetitive antagonism. Curr. Alzheimer Res. 2, 155–165. [PubMed: 15974913]

Louis RP, Lee J, and Stephenson R (2004). Design and validation of a computer-based sleep-scoring algorithm. J. Neurosci. Methods 133, 71–80. [PubMed: 14757347]

Martinez-Losa M, Tracy TE, Ma K, Verret L, Clemente-Perez A, Khan AS, Cobos I, Ho K, Gan L, Mucke L, et al. (2018). Nav1.1-overexpressing interneuron transplants restore brain rhythms and cognition in a mouse model of Alzheimer's disease. Neuron 98, 75–89.e5. [PubMed: 29551491]

Matsumoto JY, Stead M, Kucewicz MT, Matsumoto AJ, Peters PA, Brinkmann BH, Danstrom JC, Goerss SJ, Marsh WR, Meyer FB, and Worrell GA (2013). Network oscillations modulate interictal epileptiform spike rate during human memory. Brain 136, 2444–2456. [PubMed: 23803305]

Miller OH, Moran JT, and Hall BJ (2016). Two cellular hypotheses explaining the initiation of ketamine's antidepressant actions: direct inhibition and disinhibition. Neuropharmacology 100, 17–26. [PubMed: 26211972]

Mitra P, and Bokil H (2008). Observed Brain Dynamics (Oxford University Press).

Mony L, Kew JN, Gunthorpe MJ, and Paoletti P (2009). Allosteric modulators of NR2B-containing NMDA receptors: molecular mechanisms and therapeutic potential. Br. J. Pharmacol 157, 1301–1317. [PubMed: 19594762]

Mucke L, Masliah E, Yu G-Q, Mallory M, Rockenstein EM, Tatsuno G, Hu K, Kholodenko D, Johnson-Wood K, and McConlogue L (2000). High-level neuronal expression of abeta 1–42 in wild-type human amyloid protein precursor transgenic mice: synaptotoxicity without plaque formation. J. Neurosci 20, 4050–4058. [PubMed: 10818140]

Ogiwara I, Miyamoto H, Morita N, Atapour N, Mazaki E, Inoue I, Takeuchi T, Itohara S, Yanagawa Y, Obata K, et al. (2007). Nav1.1 localizes to axons of parvalbumin-positive inhibitory interneurons: a circuit basis for epileptic seizures in mice carrying an Scn1a gene mutation. J. Neurosci 27, 5903–5914. [PubMed: 17537961]

Palop JJ, and Mucke L (2016). Network abnormalities and interneuron dysfunction in Alzheimer disease. Nat. Rev. Neurosci 17, 777–792. [PubMed: 27829687]

Palop JJ, Chin J, Roberson ED, Wang J, Thwin MT, Bien-Ly N, Yoo J, Ho KO, Yu GQ, Kreitzer A, et al. (2007). Aberrant excitatory neuronal activity and compensatory remodeling of inhibitory hippocampal circuits in mouse models of Alzheimer's disease. Neuron 55, 697–711. [PubMed: 17785178]

Paoletti P, Bellone C, and Zhou Q (2013). NMDA receptor subunit diversity: impact on receptor properties, synaptic plasticity and disease. Nat. Rev. Neurosci 14, 383–400. [PubMed: 23686171]

Papadia S, and Hardingham GE (2007). The dichotomy of NMDA receptor signaling. Neuroscientist 13, 572–579. [PubMed: 18000068]

Perszyk RE, DiRaddo JO, Strong KL, Low CM, Ogden KK, Khatri A, Vargish GA, Pelkey KA, Tricoire L, Liotta DC, et al. (2016). GluN2D-containing N-methyl-d-aspartate receptors mediate synaptic transmission in hippocampal interneurons and regulate interneuron activity. Mol. Pharmacol 90, 689–702. [PubMed: 27625038]

Picard N, Takesian AE, Fagiolini M, and Hensch TK (2019). NMDA 2A receptors in parvalbumin cells mediate sex-specific rapid ketamine response on cortical activity. Mol. Psychiatry 24, 828–838. [PubMed: 30696941]

Rivolta D, Heidegger T, Scheller B, Sauer A, Schaum M, Birkner K, Singer W, Wibral M, and Uhlhaas PJ (2015). Ketamine dysregulates the amplitude and connectivity of high-frequency oscillations in cortical-subcortical networks in humans: evidence from resting-state magnetoencephalography-recordings. Schizophr. Bull 41, 1105–1114. [PubMed: 25987642]

Rubinstein M, Han S, Tai C, Westenbroek RE, Hunker A, Scheuer T, and Catterall WA (2015). Dissecting the phenotypes of Dravet syndrome by gene deletion. Brain 138, 2219–2233. [PubMed: 26017580]

Saletu B, Anderer P, and Saletu-Zyhlarz GM (2006). EEG topography and tomography (LORETA) in the classification and evaluation of the pharmacodynamics of psychotropic drugs. Clin. EEG Neurosci. 37, 66–80. [PubMed: 16733939]

Sanchez PE, Zhu L, Verret L, Vossel KA, Orr AG, Cirrito JR, Devidze N, Ho K, Yu GQ, Palop JJ, and Mucke L (2012). Levetiracetam suppresses neuronal network dysfunction and reverses synaptic and cognitive deficits in an Alzheimer's disease model. Proc. Natl. Acad. Sci. USA 109, E2895–E2903. [PubMed: 22869752]

Sapkota K, Mao Z, Synowicki P, Lieber D, Liu M, Ikezu T, Gautam V, and Monaghan DT (2016). GluN2D N-methyl-d-aspartate receptor subunit contribution to the stimulation of brain activity and gamma oscillations by ketamine: implications for schizophrenia. J. Pharmacol. Exp. Ther 356, 702–711. [PubMed: 26675679]

Saunders A, Macosko EZ, Wysoker A, Goldman M, Krienen FM, de Rivera H, Bien E, Baum M, Bortolin L, Wang S, et al. (2018). Molecular diversity and specializations among the cells of the adult mouse brain. Cell 174, 1015–1030.e16. [PubMed: 30096299]

Serraz B, Grand T, and Paoletti P (2016). Altered zinc sensitivity of NMDA receptors harboring clinically-relevant mutations. Neuropharmacology 109, 196–204. [PubMed: 27288002]

Shaffer CL, Hurst RS, Scialis RJ, Osgood SM, Bryce DK, Hoffmann WE, Lazzaro JT, Hanks AN, Lotarski S, Weber ML, et al. (2013). Positive allosteric modulation of AMPA receptors from efficacy to toxicity: the interspecies exposure-response continuum of the novel potentiator PF-4778574. J. Pharmacol. Exp. Ther 347, 212–224. [PubMed: 23899905]

Snyder EM, Nong Y, Almeida CG, Paul S, Moran T, Choi EY, Nairn AC, Salter MW, Lombroso PJ, Gouras GK, and Greengard P (2005). Regulation of NMDA receptor trafficking by amyloid-β. Nat. Neurosci 8, 1051–1058. [PubMed: 16025111]

Tai C, Abe Y, Westenbroek RE, Scheuer T, and Catterall WA (2014). Impaired excitability of somatostatin- and parvalbumin-expressing cortical interneurons in a mouse model of Dravet syndrome. Proc. Natl. Acad. Sci. USA 111, E3139–E3148. [PubMed: 25024183]

Tanahira C, Higo S, Watanabe K, Tomioka R, Ebihara S, Kaneko T, and Tamamaki N (2009). Parvalbumin neurons in the forebrain as revealed by parvalbumin-Cre transgenic mice. Neurosci. Res 63, 213–223. [PubMed: 19167436]

Texidó L, Martín-Satué M, Alberdi E, Solsona C, and Matute C (2011). Amyloid b peptide oligomers directly activate NMDA receptors. Cell Calcium 49, 184–190. [PubMed: 21349580]

Traynelis SF, Wollmuth LP, McBain CJ, Menniti FS, Vance KM, Ogden KK, Hansen KB, Yuan H, Myers SJ, and Dingledine R (2010). Glutamate receptor ion channels: structure, regulation, and function. Pharmacol. Rev 62, 405–496. [PubMed: 20716669]

Um JW, Nygaard HB, Heiss JK, Kostylev MA, Stagi M, Vortmeyer A, Wisniewski T, Gunther EC, and Strittmatter SM (2012). Alzheimer amyloid-b oligomer bound to postsynaptic prion protein activates Fyn to impair neurons. Nat. Neurosci 15, 1227–1235. [PubMed: 22820466]

van Lier H, Drinkenburg WH, van Eeten YJ, and Coenen AM (2004). Effects of diazepam and zolpidem on EEG beta frequencies are behavior-specific in rats. Neuropharmacology 47, 163–174. [PubMed: 15223295]

Vaudano AE, Ruggieri A, Avanzini P, Gessaroli G, Cantalupo G, Coppola A, Sisodiya SM, and Meletti S (2017). Photosensitive epilepsy is associated with reduced inhibition of alpha rhythm generating networks. Brain 140, 981–997. [PubMed: 28334965]

Verret L, Mann EO, Hang GB, Barth AM, Cobos I, Ho K, Devidze N, Masliah E, Kreitzer AC, Mody I, et al. (2012). Inhibitory interneuron deficit links altered network activity and cognitive dysfunction in Alzheimer model. Cell 149, 708–721. [PubMed: 22541439]

Villemure E, Volgraf M, Jiang Y, Wu G, Ly CQ, Yuen PW, Lu A, Luo X, Liu M, Zhang S, et al. (2016). GluN2A-selective pyridopyrimidinone series of NMDAR positive allosteric modulators with an improved *in vivo* profile. ACS Med. Chem. Lett 8, 84–89. [PubMed: 28105280]

Volgraf M, Sellers BD, Jiang Y, Wu G, Ly CQ, Villemure E, Pastor RM, Yuen PW, Lu A, Luo X, et al. (2016). Discovery of GluN2A-selective NMDA receptor positive allosteric modulators (PAMs): tuning deactivation kinetics via structure-based design. J. Med. Chem 59, 2760–2779. [PubMed: 26919761]

Xia P, Chen HS, Zhang D, and Lipton SA (2010). Memantine preferentially blocks extrasynaptic over synaptic NMDA receptor currents in hippocampal autapses. J. Neurosci 30, 11246–11250. [PubMed: 20720132]

Yamakawa K (2009). Molecular basis of severe myoclonic epilepsy in infancy. Brain Dev. 31, 401–404. [PubMed: 19203854]

Yang F, Snyder LB, Balakrishnan A, Brown JM, Sivarao DV, Easton A, Fernandes A, Gulianello M, Hanumegowda UM, Huang H, et al. (2016). Discovery and preclinical evaluation of BMS-955829, a potent positive allosteric modulator of mGluR5. ACS Med. Chem. Lett 7, 289–293. [PubMed: 26985317]

Yu FH, Mantegazza M, Westenbroek RE, Robbins CA, Kalume F, Burton KA, Spain WJ, McKnight GS, Scheuer T, and Catterall WA (2006). Reduced sodium current in GABAergic interneurons in a mouse model of severe myoclonic epilepsy in infancy. Nat. Neurosci 9, 1142–1149. [PubMed: 16921370]

Yuan H, Hansen KB, Zhang J, Pierson TM, Markello TC, Fajardo KV, Holloman CM, Golas G, Adams DR, Boerkoel CF, et al. (2014). Functional analysis of a de novo GRIN2A missense mutation associated with early-onset epileptic encephalopathy. Nat. Commun 5, 3251. [PubMed: 24504326]

Zajaczkowski W, Czyrak A, and Wedzony K (2003). A competitive antagonist of NMDA receptors CGP 40116 attenuates experimental symptoms of schizophrenia evoked by MK-801. Pol. J. Pharmacol 55, 703–711. [PubMed: 14704466]

Zhou Q, and Sheng M (2013). NMDA receptors in nervous system diseases. Neuropharmacology 74, 69–75. [PubMed: 23583930]

Highlights

- AD and DS mice display aberrant 12- to 20-Hz oscillations associated with epileptic spikes

- GluN2A-NMDAR enhancement reduces aberrant oscillations and spikes in AD and DS mice

- Chronic GluN2A-NMDAR activation improves cognitive functions in AD and DS mice

- GluN2A PAMs could benefit brain disorders with hypersynchrony and cognitive deficits
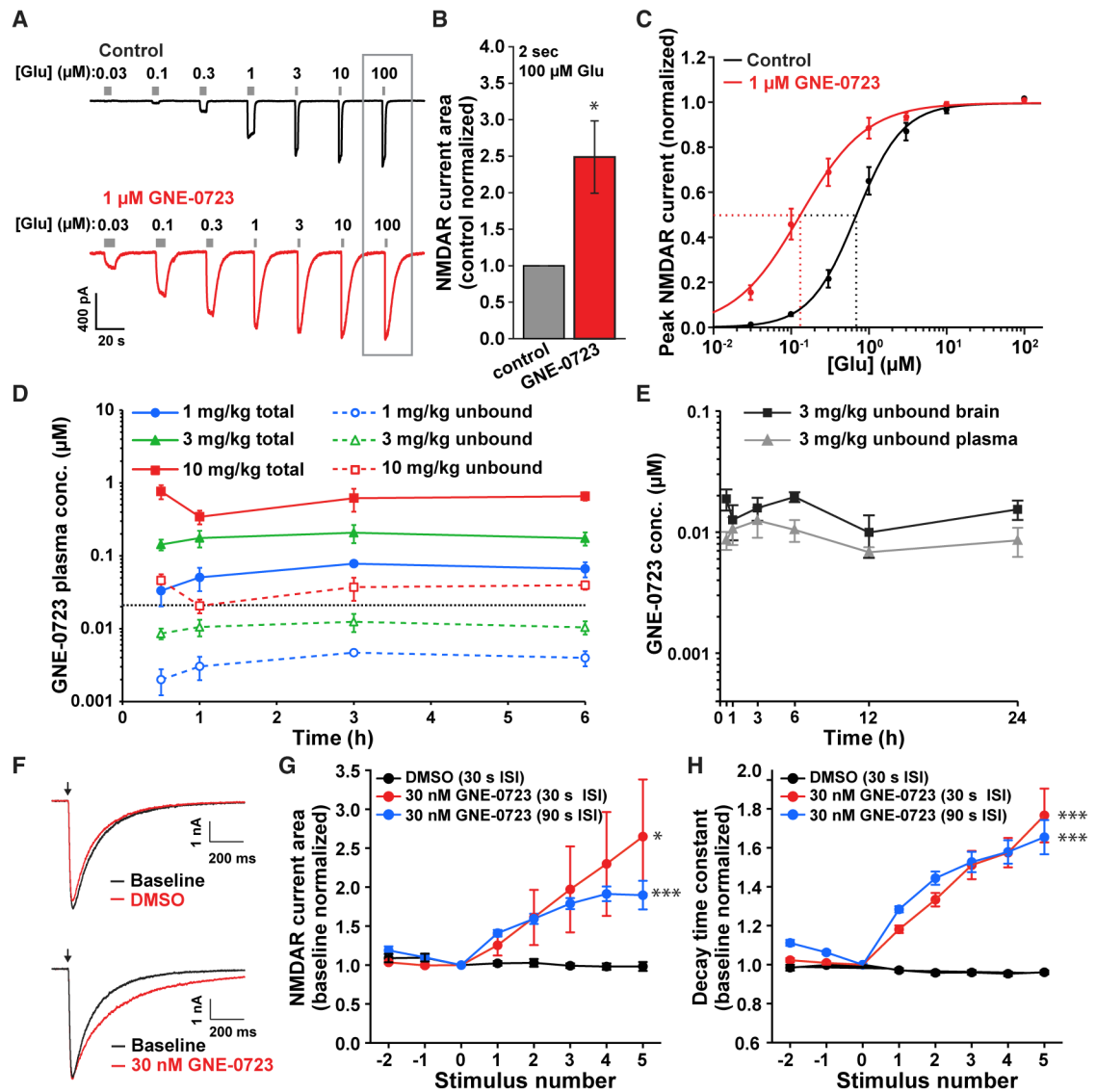
Figure 1. GNE-0723 Is an Activity-Dependent GluN2A NMDAR PAM with Suitable PK Properties for *In vivo* Use

(A) NMDAR current traces in Chinese hamster ovary (CHO) cells expressing GluN1/ GluN2A in response to pulses of increasing concentrations of glutamate (Glu) in the absence (control) or presence of 1 μM GNE-0723 (50 μM Gly was present in all solutions). Solution exchange was performed with the multichannel Dynaflow Resolve system at RT (Figure 1) or 37°C (Figure S1). To allow for potentially slow or Glu-dependent binding of GNE-0723, four consecutive 2-s pulses of 100 μM Glu were delivered in the presence of GNE-0723 (not shown) before measuring the response to different Glu concentrations.

(B) Quantification of NMDAR currents measured in response to 2-s pulses of 100 μM Glu in the absence or presence of 1 μM GNE-0723. Currents are shown normalized to the average current measured in the absence of GNE-0723. Note the significant increase in NMDA current area in the presence of GNE-0723 (n = 4/group; *p = 0.03 by Wilcoxon rank sum test).

(C) Peak NMDA current responses to increasing Glu concentrations showed a significant left shift in the EC_{50} of Glu, reflecting greater Glu sensitivity of the NMDAR in the presence of GNE-0723 (n = 4/group; p = 0.03 by Wilcoxon rank sum test). Values are shown normalized to the maximal peak current at 100 μM Glu. (D) Total and calculated unbound plasma concentrations are shown following oral dosing with 1, 3, or 10 mg/kg GNE-0723 (n = 3 mice/time point; 2 to 3 months). The dashed black line represents the GNE-0723 EC_{50} from cell-based assays (Hackos et al., 2016).

(E) Calculated unbound plasma and brain concentrations of GNE-0723 at 0.5–24 h after dosing with 3 mg/kg GNE-0723 (n = 3 mice/time point; 2 to 3 months).

(F–H) In order to more closely approximate *in vivo* synaptic activation of NMDARs, currents were recorded from the CHO cell line using piezo-electrode-controlled theta tube application of solutions. NMDAR currents were measured in response to 5-ms pulses of 100 μM Glu (arrowhead) before (top) and after (bottom) application of 30 nM GNE-0723 (50 μM Gly present in all solutions). Example traces illustrate the prominent effect of slowing of deactivation by GNE-0723, although enhancement of peak current was not evident (F). Repeated responses showed that 30 nM GNE-0723 activity-dependently potentiated NMDAR EPSC current area (G) and decay time constant (H) during repeated stimulation at 30 s or 90 s inter-stimulus intervals (ISI), indicating use dependence of GNE-0723 effects. GNE-0723 or DMSO (vehicle control) was applied after stimulus number 0. GNE-0723 significantly increased area and decay time constant of the NMDAR response measured at stimulus number 5 relative to baseline for the 30-s ISI (p < 0.05 and p < 0.001, respectively; n = 7) and 90-s ISI (p < 0.001 and p < 0.001; n = 6) conditions, but not in the DMSO condition (p = 0.78 and p = 0.36; n = 7). The amount of potentiation of the area and decay time were not significantly different between the 30-s ISI and 90-s ISI conditions (p = 0.31 and 0.24). *p < 0.05; ***p < 0.001 by Student's t test. Values are expressed as mean ± SEM (B, C, G, and H) or as mean ± SD (D and E).
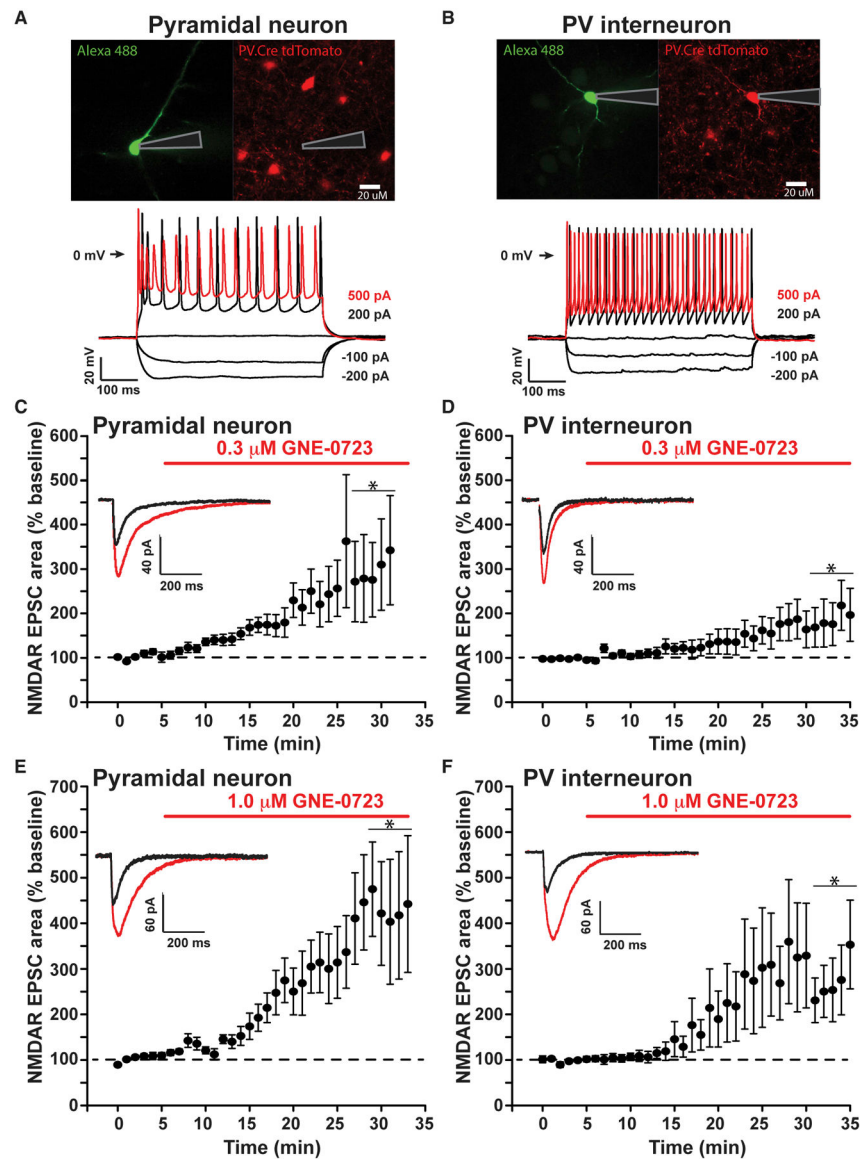
Figure 2. GNE-0723 Enhances Synaptic NMDAR Currents on Pyramidal Neurons and PV Interneurons

(A and B) Whole-cell recordings from pyramidal neurons (A) and PV interneurons (B) were made from cortical brain slices prepared from 2- to 3-month-old mice with tdTomato reporter gene expression driven by a PV-cre promoter. Neurons were filled with Alexa 488 hydrazide during recording, and neuron types were verified by morphology and electrophysiological properties. Example current clamp recordings showing typical action potential firing patterns in response to current injection are shown for each type of neuron.

(C and D) Evoked pharmacologically isolated NMDAR EPSCs were measured in pyramidal neurons (C) and PV interneurons (D) before and after application of 0.3 μM GNE-0723. Average example traces from the 5 min of baseline (black) or the last 5 min of GNE-0723 application (red) are shown inset. GNE-0723 significantly increased the average area of the NMDAR EPSC measured during the last 5 min of the experiment in the presence of the drug

compared to the 5 min before drug application in both pyramidal neurons (n = 11; p < 0.05) and PV interneurons (n = 10; p < 0.05). *p < 0.05 by Student's t test.

(E and F) NMDAR EPSCs were measured in pyramidal neurons (E) and PV interneurons (F) before (black) and after (red) application of 1.0 μM GNE-0723. GNE-0723 significantly increased the average area of the NMDAR EPSC measured during the last 5 min of the experiment in the presence of the drug compared to the 5 min before drug application in pyramidal neurons (n = 5; p < 0.05) and PV interneurons (n = 8; p < 0.05). The increasing potentiation throughout the GluN2A PAM application indicates that equilibrium receptor occupancy and maximal potentiation may not have been achieved during the time frame of these experiments, which is consistent with the use-dependent potentiation observed with recombinant NMDARs.

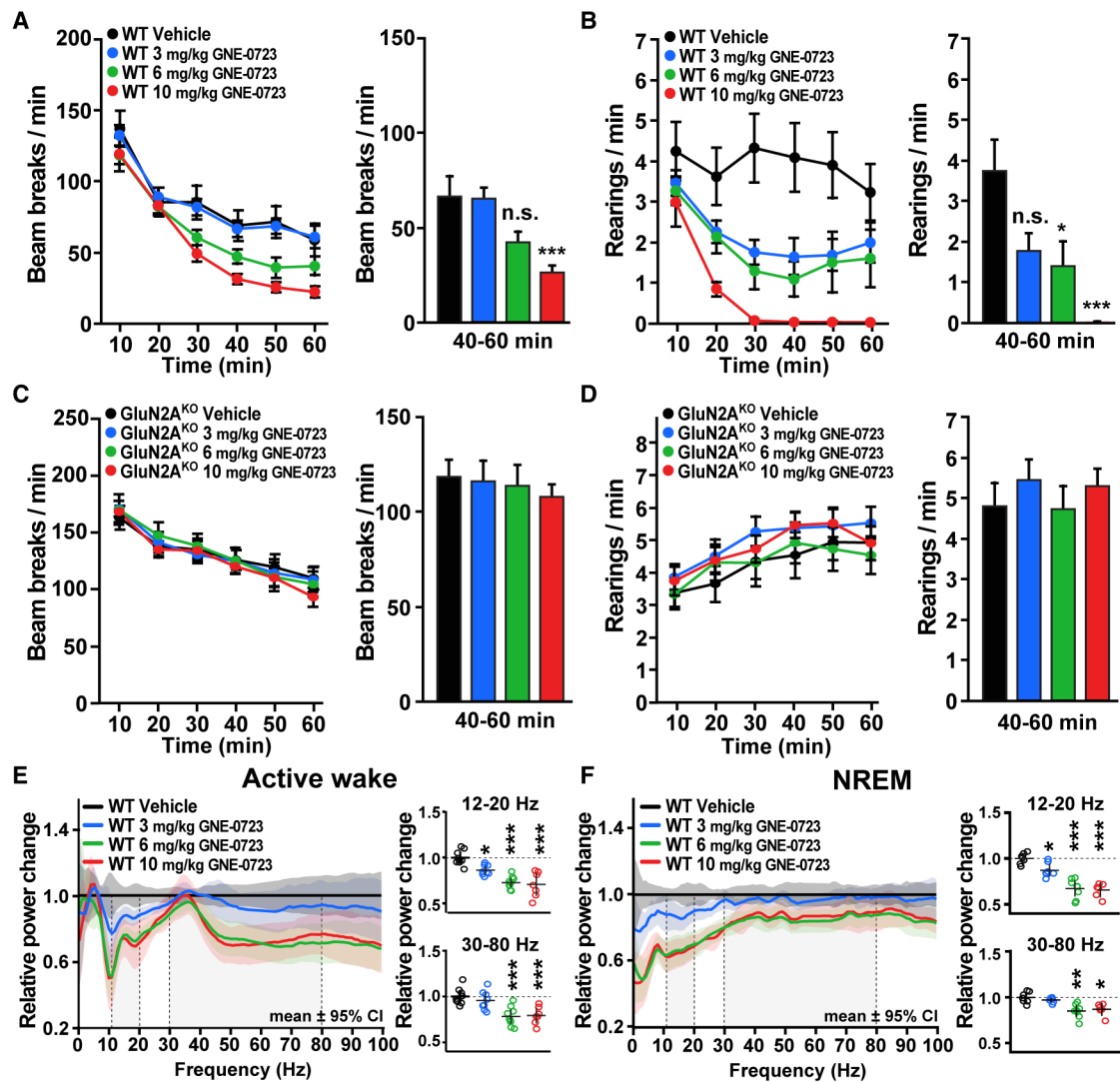All values are expressed as mean ± SEM; *p < 0.05 by Student's t test. See also Figure S1.

Figure 3. GNE-0723 Reduces Locomotor Activity in a GluN2A-Dependent Manner and Reduces EEG Oscillation Power

(A–D) Locomotor activity of sex-mixed 3- to 6-month-old GluN2A KO mice and wild-type (WT) littermate controls after treatment (time 0) with vehicle or 3, 6, or 10 mg/kg GNE-0723 (n = 13–17 per group). The number of ambulatory beam breaks and rearings are shown in 10-min bins. Bar charts show average events/min from a 30-min time window beginning 30 min after dosing (40–60 min). Higher doses of GNE-0723 treatment significantly reduced ambulatory activity (10 mg/kg; A) and rearings (6 or 10 mg/kg; B) in WT mice. *p < 0.05; ***p < 0.001 versus vehicle control by Tukey's post hoc tests. GNE-0723 treatment did not alter ambulatory activity in GluN2A KO mice (C; one-way ANOVA; p = 0.90) or rearings (D; one-way ANOVA; p = 0.71).

(E and F) EEG power across frequencies during active wake and NREM was normalized to vehicle-treated animals to assess the oscillatory effects of GNE-0723 at 3, 6, and 10 mg/kg in 2- to 3-month-old male mice. GNE-0723 at 3 mg/kg reduced 12- to 20-Hz, but not 30- to 80-Hz, oscillatory power during active wake (E) and NREM (F). Higher doses (6 and 10 mg/kg) of GNE-0723 reduced 12- to 20-Hz and 30- to 80-Hz oscillatory power during active

wake (E) and NREM (F). Vehicle = 9 (active wake) and 6 (NREM) mice; 3 mg/kg = 8 and 7; 6 mg/kg = 9 and 8; 10 mg/kg = 7 and 6, respectively). $*p < 0.05$; $**p < 0.01$; $***p < 0.001$ versus vehicle by two-way ANOVA (factors: frequency band and dose level) and Sidak's post hoc tests. See also Figures S2 and S3.

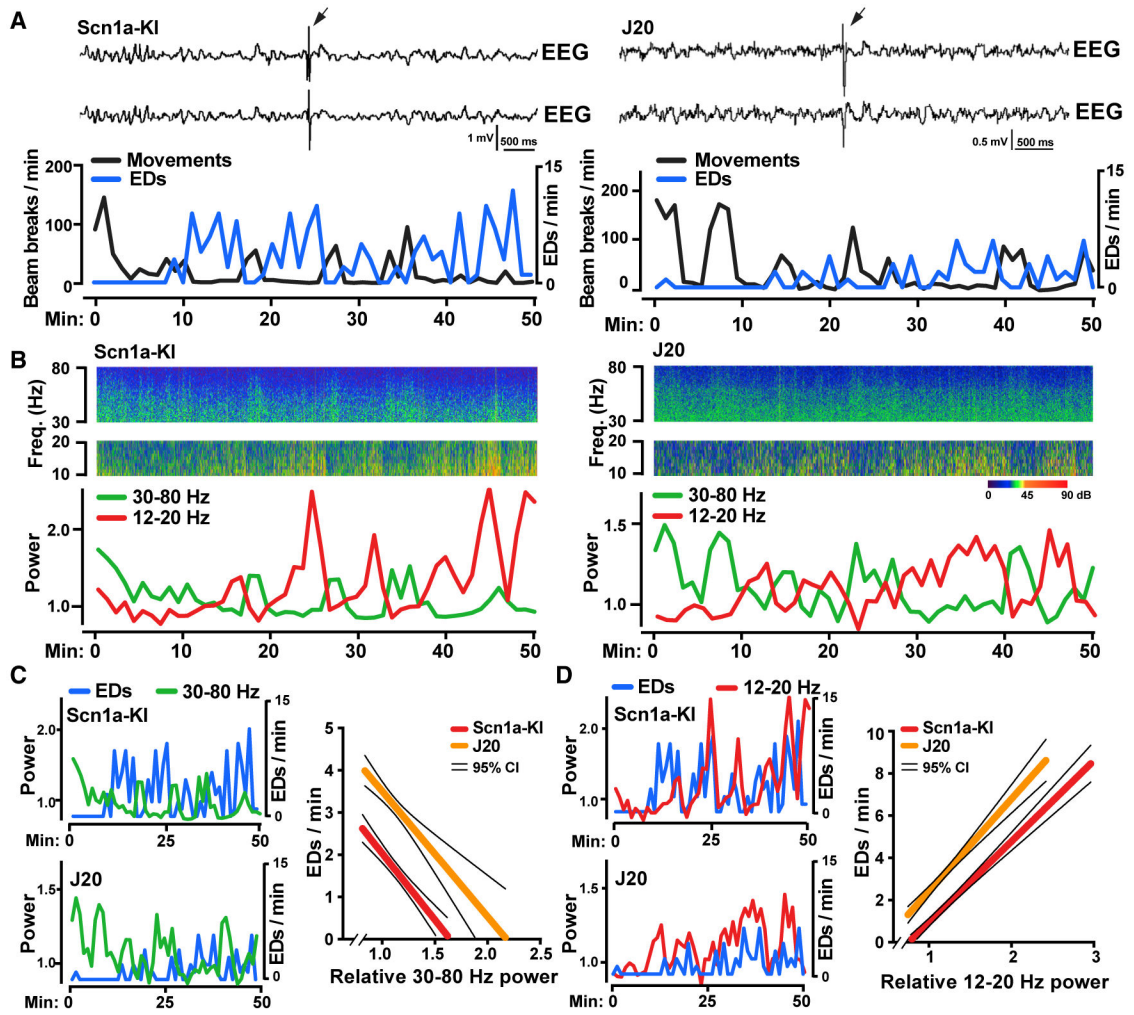Values are expressed as mean ± SEM (A–D) or mean ± 95% confidence interval (CI) (E and F).

Figure 4. Brain Oscillatory Rhythms and Behavioral Activity Are Strongly Associated with Epileptiform Activity in Scn1a-KI and J20 Mice

Oscillatory activity and epileptiform discharges (EDs) were measured for 50 min from cortical EEG recordings in sex-mixed 9- to 13-month-old Scn1a-KI (n = 10) and 7- to 11-month-old J20 (n = 18) mice (2 crossover design sessions).

(A) Traces of EEG recordings from the left and right parietal cortex (top) and movement (black, bottom) and ED rates (blue, bottom) for representative Scn1a-KI (left) and J20 (right) mice. Arrows denote EDs.

(B) EEG spectrograms (top) and oscillatory power of 12–20 Hz (red, bottom) and 30–80 Hz (green, bottom) for the same Scn1a-KI (left) and J20 (right) mice shown in (A).

(C) Traces of ED rate (blue) and 30- to 80-Hz power (green) for representative Scn1a-KI and J20 mice (left). Linear relationship between 30- to 80-Hz power and ED rate in all Scn1a-KI and J20 mice (right) is shown. 30- to 80-Hz power is negatively correlated with ED rate in Scn1a-KI and J20 mice (p < 0.001 by linear regression slope test).

(D) Traces of EDs (blue) and 12- to 20-Hz power (red) for the same Scn1a-KI and J20 mice shown in (C) (left). Linear relationship between 12- to 20-Hz power and ED rate in all Scn1a-KI and J20 mice is shown. 12- to 20-Hz power is positively correlated with ED rate in Scn1a-KI and J20 mice (p < 0.001 by linear regression slope test).
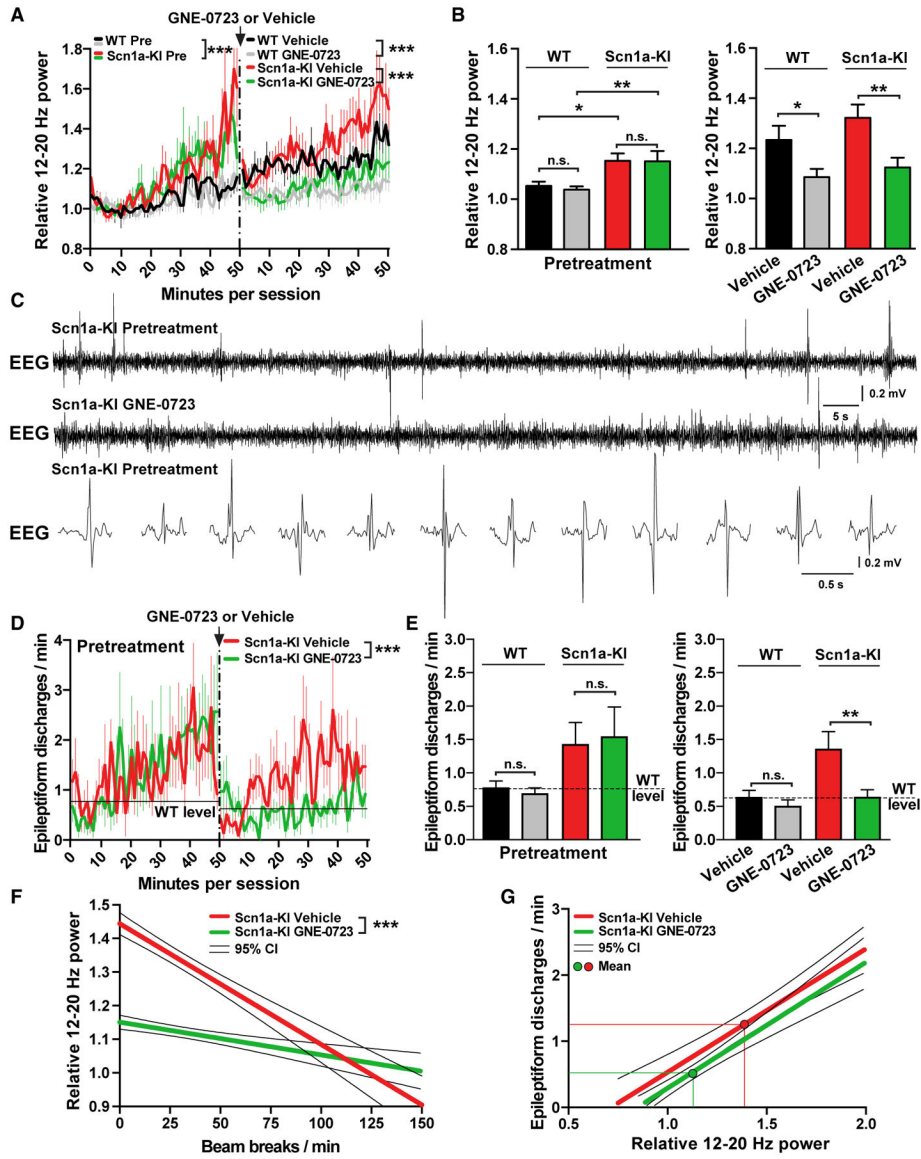
Figure 5. GNE-0723 Reduces Low-Frequency (12–20 Hz) Oscillatory Power and Epileptiform Activity in Scn1a-KI Mice

Oscillatory activity and EDs were measured from cortical EEG recordings in sex-mixed 9- to 13-month-old WT (n = 9–10) and Scn1a-KI (n = 17–19) mice during a 50- min pretreatment session and during a 50-min session beginning 30 min after administration of vehicle or 3 mg/kg GNE-0723 in a crossover design (pretreatment and treatment sessions separated by dashed line). See STAR Methods for details.

(A) Minute-by-minute 12- to 20-Hz oscillatory power during the 50 min before (pretreatment) and after vehicle or 3 mg/kg GNE-0723 treatment. During the pretreatment session, Scn1a-KI mice exhibited elevated 12- to 20-Hz power as they habituated to the open field and their exploratory activity decreased (***$p < 0.001$ by repeated-measures ANOVA and Bonferroni post hoc test for the 50-min pretreatment session). GNE-0723 significantly reduced 12- to 20-Hz power in WT and Scn1a-KI mice (***$p < 0.001$ by repeated-measures ANOVA and Bonferroni post hoc test for the 50-min treatment session).

(B) 12- to 20-Hz oscillatory power averaged over the entire pretreatment and treatment sessions. During the pretreatment session (left), both Scn1a-KI mouse groups had similar increases in 12- to 20-Hz power compared to WT control groups. 3 mg/kg GNE-0723 treatment (right) reduced 12- to 20-Hz power in WT and Scn1a-KI mice compared to vehicle-treated groups. $*p < 0.05$; $**p < 0.01$ by ANOVA and Bonferroni post hoc test.

(C) Traces of EEG recordings illustrating EDs in Scn1a-KI mice at two different temporal resolutions.

(D) Minute-by-minute ED rates before and after vehicle or 3 mg/kg GNE-0723. GNE-0723 treatment reduced EDs in Scn1a-KI mice ($***p < 0.001$ by repeated-measures ANOVA and Bonferroni post hoc test for the 50-min treatment session).

(E) ED rate averaged over the entire pretreatment and treatment sessions. During pretreatment session (left), both Scn1a-KI mouse groups had similar ED rates. 3 mg/kg GNE-0723 treatment reduced ED rates in Scn1a-KI mice. $**p < 0.01$ by Student's t test.

(F and G) 12- to 20-Hz oscillatory power as a function of locomotor activity (F) and ED rate (G) in vehicle- and GNE-0723-treated Scn1a-KI mice during the 50-min treatment session. Higher 12- to 20-Hz power strongly correlated with lower locomotor activity (F) and higher ED rate (G). GNE-0723 treatment reduced 12- to 20-Hz power particularly during periods of low locomotor activity (F; $***p < 0.001$ by linear regression analysis and slope test) but did not significantly change the tight relationship between EDs and low-frequency, 12- to 20-Hz oscillations (G).

Values are expressed as mean ± SEM (A–E) or 95% CI (F and G). See also Figure S4.
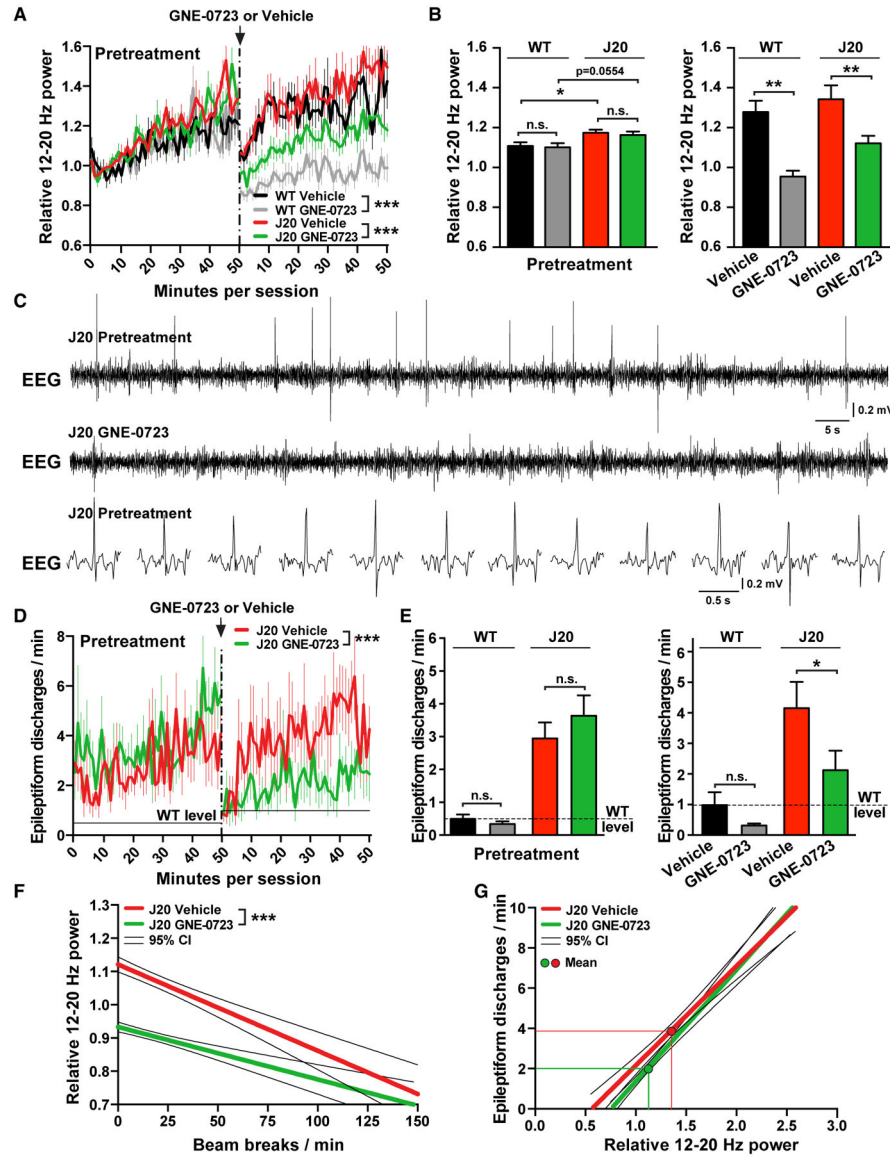
Figure 6. GNE-0723 Reduces Low-Frequency (12–20 Hz) Oscillatory Power and Epileptiform Activity in J20 Mice

Oscillatory activity and epileptiform discharges were measured from cortical EEG recordings in sex-mixed 7- to 11-month-old WT and J20 mice (n = 9 WT mice per group; n = 16–18 J20 mice per group) during a 50-min pretreatment session and during a 50-min session beginning 30 min after administration of vehicle or 3 mg/kg GNE-0723 in a crossover design (pretreatment and treatment sessions separated by dashed line). See STAR Methods for details.

(A) Minute-by-minute 12- to 20-Hz oscillatory power before and after vehicle or 3 mg/kg GNE-0723 treatment. 12- to 20-Hz power increased in all mouse groups as they habituated to the open-field arena. 3 mg/kg GNE-0723 significantly reduced 12- to 20-Hz power in WT and J20 mice (***p < 0.001 by repeated-measures ANOVA and Bonferroni post hoc test for the 50-min treatment session).

(B) 12- to 20-Hz power averaged over the entire pretreatment and treatment sessions. During the pretreatment session (left), WT and J20 mouse groups had similar 12- to 20-Hz power. During the treatment session (right), 12- to 20-Hz power increased in vehicle-treated mice but decreased in GNE-0723-treated WT and J20 mice. **$p < 0.01$ by ANOVA and Bonferroni post hoc test.

(C) Traces of EEG recordings illustrating EDs in J20 mice at two different temporal resolutions.

(D) Minute-by-minute ED rates during the 50-min pretreatment and treatment sessions. GNE-0723 treatment reduced EDs in J20 mice (***$p < 0.001$ by repeated-measures ANOVA and Bonferroni post hoc test for the 50-min treatment session).

(E) ED rate averaged over the entire pretreatment and treatment sessions. During the pretreatment session (left), both J20 mouse groups had similar ED rates. 3 mg/kg GNE-0723 treatment reduced ED rates in J2O mice. *$p < 0.05$ by Student's t test.

(F and G) 12- to 20-Hz power as a function of locomotor activity (F) and ED rate (G) in vehicle- and GNE-0723-treated J20 mice during the 50-min treatment session. Higher 12- to 20-Hz power strongly correlated with lower locomotor activity (F) and higher ED rate (G). GNE-0723 treatment reduced 12- to 20-Hz power, particularly during periods of low locomotor activity (F; ***$p < 0.001$ by linear regression analysis and slope test) but did not significantly change the tight relationship between EDs and low-frequency oscillations (G). Values are expressed as mean ± SEM (A–E) or 95% CI (F and G). See also Figure S5.
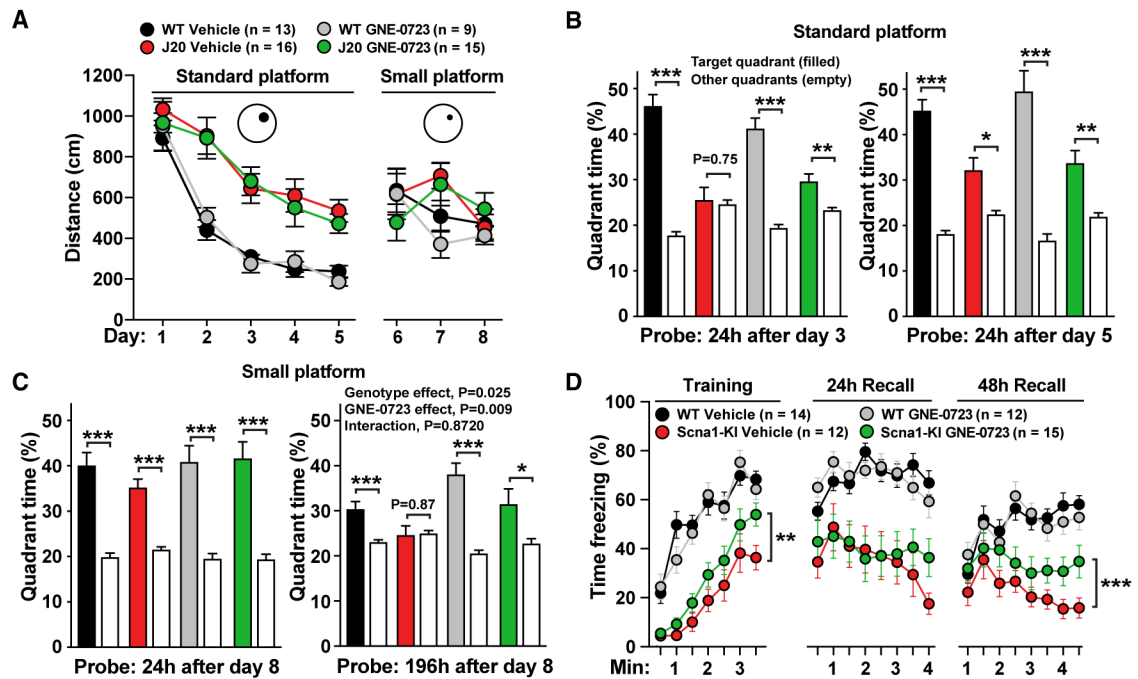
Figure 7. Chronic GNE-0723 Treatment Improves Cognitive Functions in J20 and Scn1a-KI Mice

Sex-mixed 7- to 11-month-old J20 and 10- to 12-month-old Scn1a-KI mice and their respective littermate WT controls were treated with 3 mg/kg GNE-0723 or vehicle every 48 h for at least 2 weeks before assessing cognitive performance (for J20, n = 9–13 WT and 15–16 J20 mice per treatment group; for Scn1a-KI, n = 12–14 WT and 12–15 Scn1a-KI mice per treatment group).

(A) Escape distance during the hidden platform training of the water maze test with standard (196 cm^2) and small (100 cm^2) platforms.

(B) Water maze 24-h probe trials after 3 (left) and 5 (right) days of hidden platform training with a standard platform. GEN-0723-treated, but not vehicle-treated, J20 mice had quadrant preference after 3 days of hidden platform training (left), indicating that GEN-0723 enhances spatial memory. **p < 0.01; ***p < 0.001 versus non-target quadrant locations by paired two-tailed Student's t test.

(C) 24- and 196-h probe trials after 8 days of hidden platform training in the water maze. GEN-0723-treated J20 and WT mice had stronger quadrant preference during the 196-h probe trial (right), indicating that GEN-0723 enhances long-term spatial memory. *p < 0.05; ***p < 0.001 versus non-target quadrant locations by paired two-tailed Student's t test.

(D) Percentage time freezing in the fear conditional test. Scn1a-KI mice had impaired fear learning during the training (left), 24-h recall in the same environment (middle), and 48-h recall in a similar environment (right). Compared to vehicle-treated Scn1a-KI mice, GEN-0723 treatment enhanced performance during the training and 48-h recall in Scn1a-KI mice. **p < 0.01; ***p < 0.001 by repeated-measures ANOVA and Bonferroni post hoc test. Values are expressed as mean ± SEM. See also Figure S6.

KEY RESOURCES TABLE

REAGENT or RESOURCE	SOURCE	IDENTIFIER
Chemicals, Peptides, and Recombinant Proteins		
(+)-MK-801	Tocris	Tocris Cat. # 0924
(−)-MK-801	Tocris	Tocris Cat. # 0955
GNE-0723	Pharmaron, Inc. according to methods provided in Volgraf et al., 2016	GNE-0723
Methylcellulose	Sigma Aldrich	M6385 Lot #SLBN3595V
Tween 80	Sigma Aldrich	P4780 Lot #MKBS8228V
Experimental Models: Cell Lines		
Hamster: CHO GluN1/GluN2A cells	Genentech, as described in Hackos et al., 2016	N/A
Experimental Models: Organisms/Strains		
Mouse: B6.Cg-Tg(PDGFB-APPSwInd) 20Lms/2Mmjax	Gladstone Institute of Neurological Disease	Jax stock # 34836-JAX
Mouse: Scn1aR1407X/+	Ogiwara et al., 2007	N/A
Mouse: FVB/NJ	Jackson Laboratory	Jax Stock #001800
Mouse: C57BL/6J	Jackson Laboratory	Jax Stock #000664
Mouse: tdTomato reporter	Jackson Laboratory	Jax Stock #007914
Mouse: Parvalbumin (PV)-cre	Jackson Laboratory	Jax Stock #008069
Mouse: GluN2A^{KO}	Kadotani et al., 1996	N/A